Thermal Anomalies Detect Critical Global Land Surface Changes

D. J. MILDREXLER,[a] M. ZHAO,[b] W. B. COHEN,[c] S. W. RUNNING,[d] X. P. SONG,[b] AND M. O. JONES[d,e]

[a] *Department of Forest Ecosystems and Society, Oregon State University, Corvallis, Oregon*
[b] *Department of Geographical Sciences, University of Maryland, College Park, College Park, Maryland*
[c] *Pacific Northwest Research Station, U.S. Department of Agriculture Forest Service, Corvallis, Oregon*
[d] *Numerical Terradynamic Simulation Group, Department of Ecosystem and Conservation Sciences, University of Montana, Missoula, Montana*
[e] *Department of Forest Management, University of Montana, Missoula, Montana*

(Manuscript received 7 April 2017, in final form 8 October 2017)

ABSTRACT

Measurements that link surface conditions and climate can provide critical information on important biospheric changes occurring in the Earth system. As the direct driving force of energy and water fluxes at the surface–atmosphere interface, land surface temperature (LST) provides information on physical processes of land-cover change and energy-balance changes that air temperature cannot provide. Annual maximum LST (LSTmax) is especially powerful at minimizing synoptic and seasonal variability and highlighting changes associated with extreme climatic events and significant land-cover changes. The authors investigate whether maximum thermal anomalies from satellite observations could detect heat waves and droughts, a melting cryosphere, and disturbances in the tropical forest from 2003 to 2014. The 1-km^2 LSTmax anomalies peaked in 2010 when 20% of the global land area experienced anomalies of greater than 1 standard deviation and over 4% of the global land area was subject to positive anomalies exceeding 2 standard deviations. Positive LSTmax anomalies display complex spatial patterns associated with heat waves and droughts across the global land area. The findings presented herein show that entire biomes are experiencing shifts in their LSTmax distributions driven by extreme climatic events and large-scale land surface changes, such as melting of ice sheets, severe droughts, and the incremental effects of forest loss in tropical forests. As climate warming and land-cover changes continue, it is likely that Earth's maximum surface temperatures will experience greater and more frequent directional shifts, increasing the possibility that critical thresholds in Earth's ecosystems and climate system will be surpassed, resulting in profound and irreversible changes.

1. Introduction

Earth's ecosystems are experiencing change that is unprecedented in human history (Steffen et al. 2007; IPCC 2013). These changes, primarily driven by humanity's expanding land-use footprint and increasing global emissions of atmospheric greenhouse gases, threaten to initiate potentially irreversible changes in the Earth system (Rockström et al. 2009; Hansen et al. 2012). For example, investigations into the effects of climate change on the cryosphere have implicated increasing temperatures in the melting of glaciers and thinning of ice sheets, and the Greenland Ice Sheet (GrIS) has been one of the largest contributors to global sea level rise over the past 20 years (Lenaerts et al. 2013; Khan et al. 2014; Yin et al. 2011; McMillan et al. 2016). In tropical forests the persistent effects of increasingly severe droughts, decreases in rainfall, and the interactions with ongoing forest loss suggest the potential for large-scale degradation of these forests (Malhi et al. 2008; Marengo et al. 2011; Saatchi et al. 2013; Hilker et al. 2014; Zhou et al. 2014). An urgent goal of Earth science research today is the development of indicators to measure global changes and their consequences on climate that are relevant and communicable to society and decision-makers (Janetos et al. 2012). Land surface temperature (LST) is one of the most important parameters in the physical processes of surface energy and water balances from local through global scales (Mannstein 1987; Li et al. 2013; Wan et al. 2004). Its retrieval from remotely sensed thermal infrared data provides spatially continuous LST measurements with global coverage to examine the thermal heterogeneity of

Corresponding author: David Mildrexler, d.mildrexler@gmail.com

DOI: 10.1175/JAMC-D-17-0093.1

Earth's surface and the impact on surface temperatures resulting from natural and human-induced changes (Jin and Dickinson 2010; Li et al. 2015). Here, we present a new global-change indicator that is based on an annual global measure of Earth's maximum LST (LSTmax) and demonstrate its value to examine critical functions of the Earth system. We investigate whether maximum thermal anomalies could be indicative of heat waves and droughts, a melting cryosphere, and tropical-forest disturbance.

Whereas the focus of analyses of global temperature is usually on air temperature (IPCC 2013; Hansen et al. 2006), LST provides a more direct measure of the surface conditions and is the more relevant quantity to measure when analyzing surface–climate interactions (Li et al. 2013). LST measures the emission of thermal radiance from the actual land surface where the incoming solar energy interacts with and heats the ground or, in vegetated areas, the surface of the canopy. This quality makes LST a good indicator of energy partitioning at the land surface–atmosphere boundary and sensitive to changing surface conditions (Nemani et al. 1996; Wan et al. 2004; Lambin and Ehrlich 1995; Mildrexler et al. 2009). By comparison, the standard weather-station air temperature is measured 1.5 m above the ground level with sensors protected from radiation and adequately ventilated (Pielke et al. 2007). Because air is such a poor heat conductor, as midsummer temperatures go up and more thermal energy is concentrated at Earth's surface, LST increases more rapidly than the corresponding air temperature (Mildrexler et al. 2011a). LST is more closely connected to the biophysical characteristics of the land surface, such as the land-cover type, vegetation density, and water and energy fluxes of a specific area, than is air temperature (Oyler et al. 2016). Moreover, weather stations have an inequitable global distribution, including few stations across remote areas of Earth's land surface, and cannot give detailed spatial patterns (Kogan 1997; Daly et al. 2008; Mu et al. 2013; Li et al. 2015). For example, in this study we examine ice sheets and rain forests because of their importance in the global climate system. With the Moderate Resolution Imaging Spectroradiometer (MODIS) sensor on board the *Aqua* satellite, LST is measured at every 1-km pixel across the 1.7×10^6 km^2 of the Greenland ice sheet. By comparison, the Greenland Climate network consists of 18 weather stations at which air temperature is recorded, that is, approximately 1 station for every 94 000 km^2. Such a small number of monitoring stations limits our ability to understand what is happening across the entire area. The same is true for other remote regions of Earth such as the Amazon and Congo rain forests, where sparse weather-station coverage limits monitoring capability (see Fig. 1 in Mildrexler et al. 2011a), whereas remotely sensed LST provides spatially exhaustive coverage. These differences allow LST to magnify the land surface dynamics in a way that air temperatures cannot, offering a new and unique measure of biospheric change.

In recent decades an increase in the frequency and the total land area affected by extreme-high-temperature events such as droughts combined with heat waves has been linked to global warming (Seneviratne et al. 2014; Perkins et al. 2012). Extremely hot summertime outliers that once covered 1% of Earth's land area now cover about 10% of the land area (Hansen et al. 2012). Such extremes amplify moisture deficit and heat stress and result in an increase in tree mortality and wildfire (Allen et al. 2015; Mitchell et al. 2014; Teskey et al. 2015; Mildrexler et al. 2016). The frequency and severity of extreme droughts and heat waves are predicted to increase in the future (Cook et al. 2014; IPCC 2013; Jentsch et al. 2007; Mitchell et al. 2014; Moritz et al. 2012; Fischer and Schär 2010). The global increase in high-temperature-related extreme events portends the potential for regional-scale transitions in land cover once physical and/or physiological thresholds are surpassed, some of which are critical thresholds in the global climate system (Grimm et al. 2013; Chapin et al. 2008; Christidis et al. 2015). For instance, the cryosphere's ice- and snow-covered surfaces have extremely cold LSTmax values and play an important role as a climate buffer through the physics of phase change (Kenney and Janetos 2014). As ice sheets are exposed to warmer conditions, increased surface melt lowers the albedo, resulting in increased absorption of solar radiation and a positive feedback with further temperature increase and more surface melt (Tedesco et al. 2011; He et al. 2013). Tropical-forest ecosystems are critical in cooling Earth's surface temperatures, contain large stores of carbon, support tremendous biological diversity, and, in this century, face the dual threats of forest clearing and stress from climate change (Lee et al. 2011; Li et al. 2015; Malhi et al. 2008; Marengo et al. 2011). Climate-model predictions indicate that extremely dry events may increase with climate change, pushing tropical forests toward a climatically induced tipping point and possible biome-level degradation (Cox et al. 2004; Malhi et al. 2009). Here, we utilize the high-resolution and spatially continuous global coverage of the LST data to 1) examine LSTmax anomalies and their association with verified heat waves and droughts from 2003 to 2014, 2) monitor large-scale ice warming and phase-change-driven temperature shifts in the cryosphere, and 3) investigate changes in surface temperatures in evergreen broadleaf forests (EBF) in accordance with the 2005 and 2010 droughts and in response to forest loss.

The uniqueness of annual maximum LSTs

Multiple lines of research have found that the daytime LSTmax from the *Aqua* MODIS sensor is a unique and informative annual monitoring metric for integrating the biophysical influence of land cover and the consequences of changes across Earth's land surface. The *Aqua* satellite's equatorial afternoon overpass time of approximately 1330 allows for near-ideal retrievals of maximum daily LST because it is temporally coincident with the maximum daily temperature of the land surface (Sinclair 1922; Wan et al. 2004; Coops et al. 2007). The *Aqua* MODIS LST measurements capture the thermal response of rising leaf temperatures that result from decreased latent heat flux as stomata close and soil litter surfaces dry, accentuating differences in LST among vegetation cover types (Mildrexler et al. 2007). Focusing on Earth's maximum surface temperatures provides important insights into the extremes of high temperature that are associated with droughts and heat waves and the thermal tolerances and exposures for different biomes and species (Wan et al. 2004).

Satellite-derived LST is influenced by synoptic weather variability (wind speed, cloud cover, humidity, radiation loading, etc.) on a continual basis and has high natural variability (Friedl and Davis 1994; Nemani and Running 1997). Although temperatures over land surfaces generally vary strongly in space and time (Prata et al. 1995; Li et al. 2013), annual-maximum-value compositing removes the natural synoptic variability that is associated with daily–seasonal LST while focusing on the maximum temperature in a given area. For a specific location and in the absence of change, the LSTmax metric has relatively low interannual variability such that deviations are indicative of large-scale ecological-disturbance events (Mildrexler et al. 2009). Moreover, the timing of LSTmax generally occurs during the year's driest clear-sky conditions. This, in turn, imposes a strong limitation on the partitioning among the sensible and latent heat fluxes (H and LE, respectively) that largely control the surface temperature in the surface energy balance (Bateni and Entekhabi 2012; Sandholt et al. 2002). Thus, LSTmax measurements provide unique information on how the partitioning between H and LE varies and affects the expression of LSTmax across Earth's surface in this moisture-limited condition. The vegetated fraction of Earth's surface has important effects on the magnitude and relative partitioning of the turbulent fluxes (H + LE) because plants are the primary site for the exchange of water, energy, and momentum between the land and the atmosphere. Indeed, a strong relationship has been observed between LSTmax and vegetation density over a wide range of land-cover types (Mildrexler et al. 2007; Nemani et al. 1993; Goward et al. 1985; Smith and Choudhury 1991; Sandholt et al. 2002; Coops et al. 2007). The variations in land surface properties and vegetation densities across Earth's surface give LSTmax a unique biogeographic influence (Fig. 1). For example, forests, with their relatively deep root systems, can tap groundwater even during dry conditions and, through transpiration, partition a larger proportion of incoming solar radiation to LE, cooling their surface temperature relative to other land-cover types (Mildrexler et al. 2011a).

The complete global coverage and 1-km^2 resolution of the LST data provide detailed spatial information that can be examined at local (Zhou et al. 2012), regional (Jin and Mullens 2012; Van De Kerchove et al. 2013), and global scales (Mildrexler et al. 2011b; Li et al. 2015). Spatially continuous global LSTmax maps provide the means to visually assess the patterns of the highest temperatures across both large-scale gradients of natural vegetation density and type (Figs. 1a,b)—such as the transition from the tropical rain forests of the Congo to the Sahara Desert—and relatively small-scale land-cover changes resulting from irrigation and urban development. This scalability facilitates focusing on different regions of Earth's land surface to explore the driving factors of change that contribute to the integrated global measurement. LSTmax has the potential to indicate large-scale shifts in Earth's biosphere while also retaining its physical meaning and significance across every 1-km^2 pixel of Earth's land surface, an important distinction from air-temperature-based indicators.

The pixel-specific standard deviations (SD) from the 12 years of LSTmax data show interesting variations across Earth's surface (Fig. 1c). Relatively low standard deviations are found in the EBF, ice/snow, and barren cover types. Grasslands, croplands, and shrublands represent the LSTmax pixels with the highest standard deviations. The land-cover-aggregated mean LSTmax and standard-deviation values support these observations and provide insights into the biophysics of different land-cover types during thermal maximum (Fig. 1d). For example, barren areas have the highest mean LSTmax of any cover type (51.9°C) and the lowest standard deviation (1.27°C) as a result of the routine hot and dry climatic conditions during summer when LSTmax occurs and the bare soil surfaces that result in extreme high surface temperatures. Ice/snow areas have the lowest mean LSTmax (−12.2°C) and the second lowest standard deviation (1.32°C). This result is mainly attributable to the high albedo of ice/snow environments that results in consistently low LSTmax values. Forests have some of the lowest mean LSTmax values of all of the vegetated biomes, and EBF is unique among forest types for its low standard deviation (Fig. 1d). This result

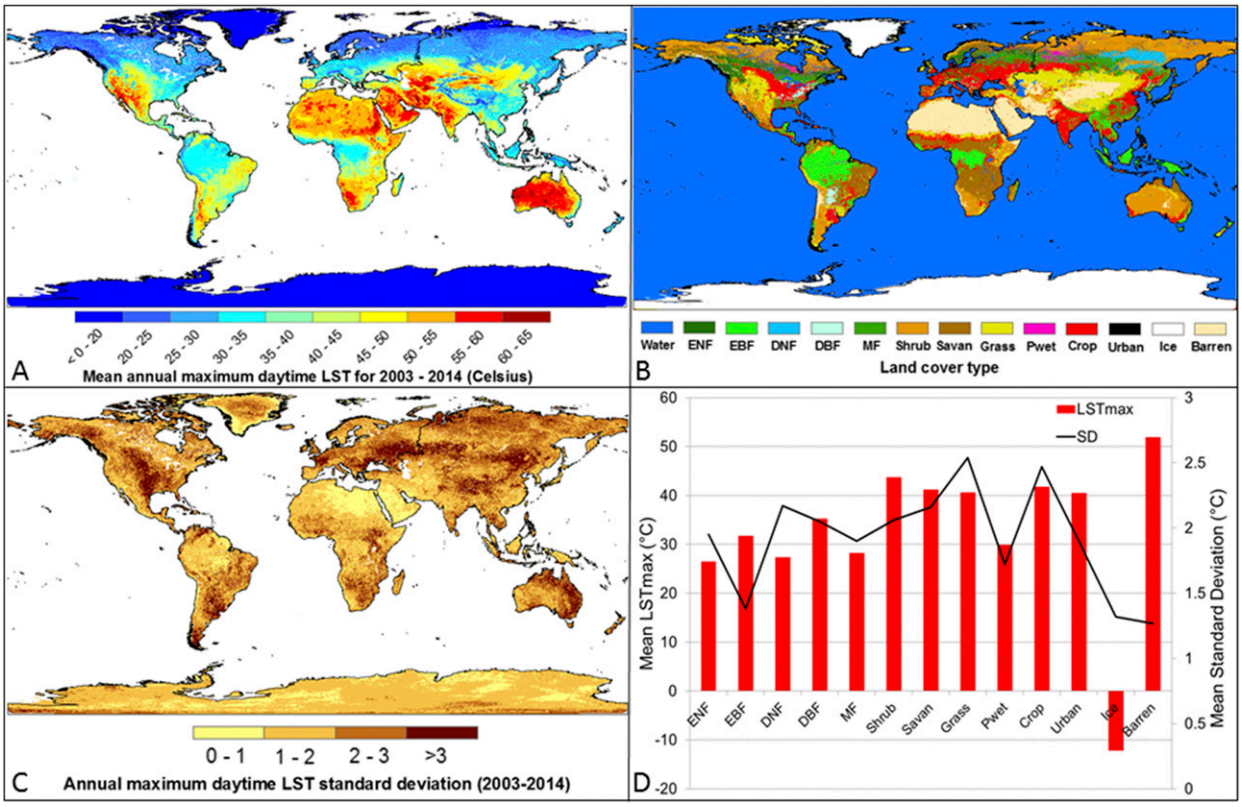

FIG. 1. (a) Continuous global map of LSTmax from 2003 to 2014. (b) The 2003 MODIS Land Cover dataset (Friedl et al. 2010) with classification-system abbreviations defined as evergreen needleleaf forest (ENF), evergreen broadleaf forest (EBF), deciduous needleleaf forest (DNF), deciduous broadleaf forest (DBF), mixed forests (MF), shrublands (Shrub), savannas (Savan), grasslands (Grass), permanent wetlands (Pwet), croplands (Crop), and ice/snow (Ice). Note that we combined open and closed shrublands into shrub, and woody savanna and savanna into Savan. (c) The pixel-specific standard deviations (SD) from 2003 to 2014. (d) Mean LSTmax and mean SD by land-cover type [same abbreviations as in (b)].

likely reflects year-round access to moisture and tighter regulation of surface temperature through transpirational cooling in the EBF cover type. Grasslands grow in relatively mild climates and have the capacity for large and rapid productivity response to variation in precipitation (Knapp and Smith 2001; Holmgren et al. 2006; Mildrexler et al. 2007), resulting in greater variation in the expression of LSTmax (Fig. 1d).

The annual LSTmax histograms include every 1-km^2 pixel across the global land surface and display a distinctive multimodal distribution that is influenced by the biophysical and biogeographic factors of Earth's ecosystems (Fig. 2). Ice/snow areas account for the low-temperature mode (approximately from −30° to 0°C), including the high kurtosis at 0°C, the melting point of ice. The central mode of the global histogram (~20°–35°C) is driven by forest land-cover types, and high-latitude shrublands in the Northern Hemisphere also fall within this temperature range. Grasslands, croplands, and some savannas have relatively warm mean LSTmax values and are integrated within the 30°–50°C temperature range of the global histogram (Fig. 2). Barren deserts and shrublands in hot, dry environments are reflected in the high-temperature mode (~50°–65°C)

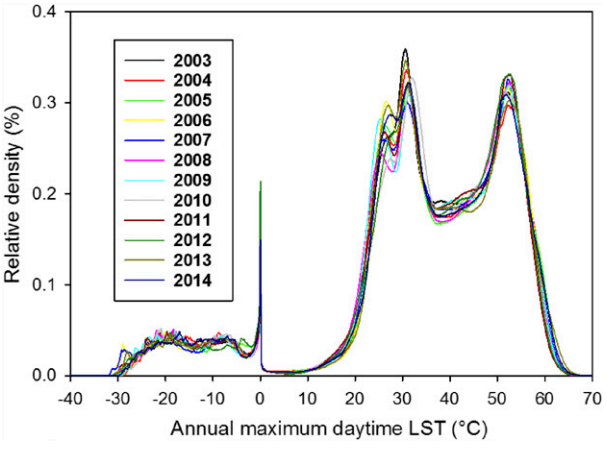

FIG. 2. The global maximum thermal signature of Earth's land surface from 2003 to 2014. The area under the annual density curves sums to 1.

of the histogram. The annual global LSTmax histograms illustrate that Earth has a unique maximum thermal signature and the same general distribution across 12 years of LSTmax data, reflecting two important global-scale land surface dynamics. First, in any given year, the vast majority of Earth's land surface is undisturbed (Potter et al. 2003; Mildrexler et al. 2009; Goward et al. 2008). Second, the aggregate effects of natural disturbances globally on the surface energy balance, such as from the loss of vegetation to fire and the regrowth from natural succession, act to average each other out (Bowman et al. 2009). By starting from this integrated global perspective, we have developed an understanding that bulk shifts in any component of the histogram signal potential major climate or human-induced changes in the Earth system. Using the MODIS Land Cover (see section 2b) results as a mask, LSTmax data can be extracted for specific cover types and land-cover-specific histograms can be analyzed for change.

2. Data and methods

The key datasets used in this study are global satellite-derived LST and land-cover data from the MODIS sensor from 2003 to 2014. We also used Landsat-derived forest-loss data and continental perimeter maps for classification and comparison of the LST data. Our approach involves several key steps: 1) annual-maximum-value compositing of the 1-km^2 LST data and calculation of LSTmax annual histograms, 2) calculation and spatial analysis of the global LSTmax pixel-specific standardized anomalies and their association with verified heat waves and droughts, 3) calculation of ice/snow LSTmax histograms and examination of interannual variations and spatial patterns related to ice melt in Greenland and Antarctica, and 4) calculation of EBF LSTmax histograms and examination of interannual shifts and anomalies that are associated with drought and forest loss in South America and Africa, where the EBF forest area is predominantly within the Amazon and Congo rain forests, respectively.

a. Aqua *MODIS LST data*

We used the collection-5 *Aqua* MODIS 8-day daytime LST ("MYD11A2") from 2003 to 2014 at 1-km^2 spatial resolution. The MODIS LST products have been validated to within 1 K at multiple sites in relatively wide ranges of surface and atmospheric conditions (Wan et al. 2004; Wan 2008). Refinements to the collection-5 LST product have minimized the main sources of uncertainty caused by cloud contamination and in accurately estimating the surface emissivity and have significantly improved the accuracy and stability of the MODIS LST products (Wan 2008). Annual-maximum-value compositing was applied to the LST data, selecting independently for each pixel the maximum 8-day LST over a 1-yr period from all 8-day composites labeled as reliable by the MODIS quality control and combined into one seamless image representing the highest LST recorded at every 1-km^2 pixel on Earth's surface for a given year. LSTmax has been used to pinpoint global hot spots (Mildrexler et al. 2011b), to map large-scale ecological disturbances and human-induced land-cover change at regional and continental scales (Lambin and Ehrlich 1995; Li et al. 2015; Mildrexler et al. 2007, 2009), to examine the degree to which different land-cover types regulate LSTmax and how it varies in comparison with air temperature globally (Mildrexler et al. 2011a), and to better understand the maximum thermal characteristics of the global land surface (Mildrexler et al. 2011b).

LSTMAX STANDARDIZED ANOMALY MAPS

Biophysical data such as LST are easily interpreted as a relative anomaly, that is, a departure from a baseline condition (Janetos et al. 2012). The LSTmax anomaly is calculated on an annual basis as pixelwise anomalies from each pixel's long-term-data-record mean (2003–14):

$$\mathrm{LSTmaxAnomaly}_{\mathrm{annual}} = \mathrm{LSTmax}_{\mathrm{current\_year}} - \mathrm{LSTmax}_{\mathrm{data\_record\_mean}}. \quad (1)$$

The LSTmax anomalies are calculated relative to the 2003–14 average, with normal being the 0 point. We then used the LSTmax anomalies to compute the pixel-specific standardized anomaly, which gives the anomaly relative to each pixel's variance (Grumm and Hart 2001):

$$\mathrm{LSTmaxStandardAnomaly}_{\mathrm{annual}} = \mathrm{LSTmaxAnomaly}_{\mathrm{annual}}/\mathrm{standard\ deviation}. \quad (2)$$

The standardized anomaly increment represents the number of standard deviations by which the anomaly departed from normal, providing information on the relative significance of anomalous features and how they vary across different land-cover types (Grumm and Hart 2001).

b. MODIS Land Cover data

The MODIS collection-5.1 Land Cover product (''MCD12Q1'') provides annually updated land-cover maps with a spatial resolution of 1 km^2 (Cai et al. 2014). Because the primary objective of the MODIS Land Cover product is to facilitate the inference of biophysical information for use in regional and global modeling studies, it must therefore be discernible with high accuracy and directly related to physical characteristics of the surface, especially vegetation (Friedl et al. 2002). A classification scheme developed by the International Geosphere–Biosphere Programme groups Earth's surface into 17 major classes. This scheme provides a consistent grouping method to compute the land-cover-specific LSTmax statistics and to provide biophysical interpretation. We used land-cover-specific masks to extract the annual LSTmax and anomaly data for specific cover types and to develop cover-specific histograms. To reduce uncertainties related to annual changes in the land-cover map, we used the land-cover data from 2003 to match with our first full year of *Aqua* MODIS LST data and held this layer constant for all other years (2003–14).

c. Forest-loss data

Forest loss was derived from 30-m^2-spatial-resolution Landsat-based annual forest-change data (Hansen et al. 2013). Forest losses from 2000 to 2012 were aggregated from 30 m to 1 km in a sinusoidal projection and were mosaicked to global ''geotiff'' files. Each change layer gives the percentage of Landsat forest-change pixels that experienced forest loss during each year within a 1-km grid. Cumulative losses were computed as the total percentage of forest-cover loss that occurred between 2000 and 2012. To examine the effects of significant large-scale forest loss on LST in the EBF cover type, we used a threshold of 30% forest loss, indicating that at least 30% of the MODIS 1-km pixel had experienced forest loss during the study period. This threshold has proven to be effective for detecting the majority of abrupt disturbances (e.g., logging) across the 1-km MODIS pixel (Sulla-Menashe et al. 2014). To examine the effect of forest loss on LSTmax, we utilized two approaches. First, to determine whether persistent increases in the LSTmax of EBF were associated with areas that experienced forest loss, we computed the mean temperature change between the first (2003–08) and second (2009–14) halves of the study period (globally and for South America) at each pixel and then compared the changes with areas that experienced greater than 30% forest loss from 2002 to 2012. Second, we compared the temperature change for pixels that experienced greater than 30% forest loss with those that experienced less than 30% forest loss between the first year (2003) and the last year (2014) of our study period. Given our interest in LSTmax change across the study period and the persistent multiyear effects of forest loss on LSTmax change, the minor temporal offset of the LSTmax and forest-loss datasets was not a concern.

3. Results

a. Global heat waves

Strong positive and negative anomalies were detected across the global land surface from 2003 to 2014 (Fig. 3). We used the spatially continuous LSTmax anomaly data to monitor for extreme heat events from 2003 to 2014 and found that positive anomalies correspond to major droughts and heat waves during every year of the study period and on every continent on Earth (Table 1). Area affected by positive anomalies peaked in 2010 and 2012 when 20% and 19%, respectively, of the global land area experienced anomalies greater than 1 SD and more than 4% and 3%, respectively, of the total area were subject to severe positive anomalies (>2 SD) (Fig. 4). The 2010 peak coincides with widespread heat waves and droughts in Russia, Kazakhstan, Mongolia, and China (Sun et al. 2014) and in the Amazon and Congo rain forests (Marengo et al. 2011; Zhou et al. 2014). In 2012, positive LSTmax anomalies stretched across the Northern Hemisphere in accordance with summer heat waves and drought in North America (Wang et al. 2014; Cattiaux and Yiou 2013; Karl et al. 2012) and northern Eurasia (Schubert et al. 2014). The 2012 positive anomaly over Greenland was the most extreme melt year ever recorded across the GrIS with satellite monitoring (Nghiem et al. 2012).

A focus on two high-profile heat waves reveals the complex spatial patterns and the magnitude of LSTmax anomalies associated with the 2003 European heat wave and the 2010 Siberian heat wave (Fig. 5). The most intense anomalies exceeded 2.5 SD for both events, with a few pixels in excess of 3 SD. In both features, these intense anomalies display a patchy spatial pattern, connected by positive anomalies of varying intensity. The overall expression of positive anomalies together gives a spatially defined footprint of the heat waves' most extreme surface temperatures. These anomalous features show interesting spatial variations, including interior patches and complex edge effects with nonsignificant anomalies (<1.0 SD), most notably in the 2003 European heat wave. These heat waves were associated with continent-wide reductions in ecosystem productivity (Ciais et al. 2005; Zhao and Running 2010; Schwalm et al. 2012), heat-stress-induced damages to natural and agricultural systems (Cattiaux and Yiou 2013; Bréda et al. 2006;

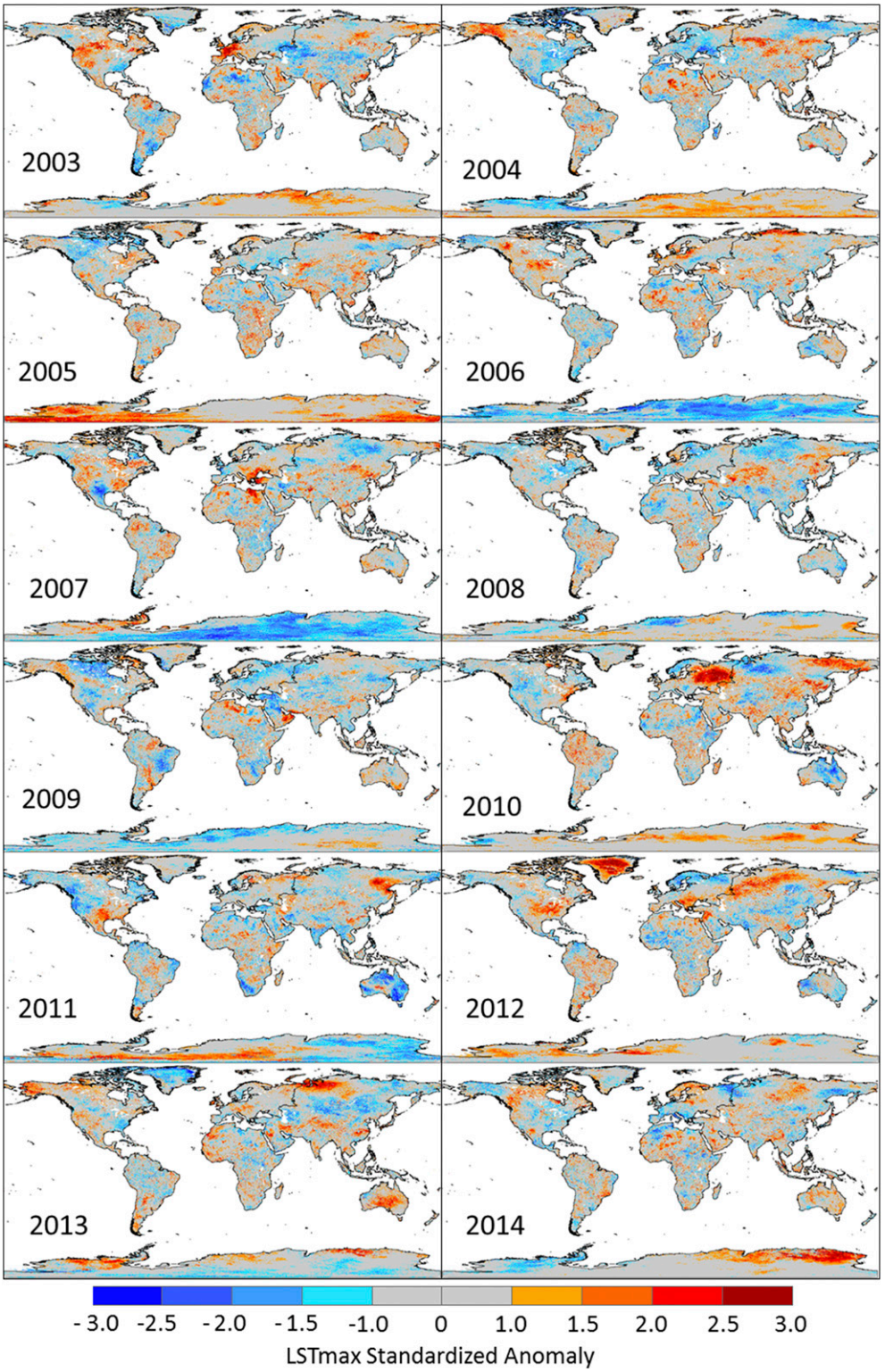

FIG. 3. Spatial extent and severity of LSTmax standardized annual anomalies from 2003 to 2014.

TABLE 1. Documented cases of drought and/or heat waves detected from 2003 to 2014.

Location	Year	Reference(s) and/or URL
Europe	2003	Rebetez et al. (2009); Stott et al. (2004)
Western United States	2003	Bumbaco and Mote (2010)
Alaska	2004	Wendler et al. (2011)
Southern Asia	2005	http://earthobservatory.nasa.gov/IOTD/view.php?id=5603
East Africa	2005	Hastenrath et al. (2007)
Amazon	2005	Marengo et al. (2008)
Antarctica	2005	Bromwich et al. (2013)
North America	2006	http://www.noaanews.noaa.gov/stories2006/s2759.htm
Europe	2006	Fouillet et al. 2008; Rebetez et al. (2009)
Australia	2006	http://www.bom.gov.au/climate/current/month/aus/archive/200611.summary.shtml
North America	2007	Fuhrmann et al. (2011)
Southern Europe	2007	Coumou and Rahmstorf (2012); Founda and Giannakopoulos (2009)
Eastern United States	2008	https://web.archive.org/web/20120915133242/http://nws.met.psu.edu/severe/2008/09Jun2008.pdf
Southeastern Australia	2009	Coumou and Rahmstorf (2012); Karoly (2009); http://www.bom.gov.au/climate/current/statements/scs17d.pdf
La Plata basin, South America	2009	Chen et al. (2010); http://www.ipsnews.net/2009/01/agriculture-argentina-worst-drought-in-100-years/
Russia; eastern Europe	2010	Barriopedro et al. (2011); Grumm (2011)
Quebec, Ontario, Canada	2010	Bustinza et al. (2013)
Brazil	2010	Marengo et al. (2011)
Congo rain forest	2010	Zhou et al. (2014)
Texas and Oklahoma	2011	Hoerling et al. (2013); Hansen et al. (2012); Coumou and Rahmstorf (2012); Long et al. (2013)
United States	2012	Cattiaux and Yiou (2013); Karl et al. (2012); Wang et al. (2014)
Greenland	2012	Nghiem et al. (2012); Neff et al. (2014)
Russia	2012	https://www.oxfam.org/sites/www.oxfam.org/files/cs-russia-drought-adaptation-270913-en.pdf
Eurasia	2012	Schubert et al. (2014)
Australia	2013	Lewis and Karoly (2013); http://www.bom.gov.au/climate/current/annual/aus/2013/
Ireland; United Kingdom	2013	Elliot et al. (2014); http://www.metoffice.gov.uk/news/releases/archive/2013/warm-july-stats
Alaska	2013	http://cms.met.psu.edu/sref/severe/2013/18Jun2013.pdf
Eastern China	2013	http://news.xinhuanet.com/english/indepth/2013-08/13/c_132627590.htm
Argentina	2013	http://www.bbc.com/news/world-latin-america-25564633
Northern Europe	2014	Baker-Austin et al. (2016); http://en.ilmatieteenlaitos.fi/press-release/42503751
Australia	2014	http://www.bom.gov.au/climate/current/statements/scs48.pdf
British Columbia, Canada; northwestern United States	2014	http://www.cbc.ca/news/canada/british-columbia/b-c-heat-wave-3-hottest-spots-and-20-records-broken-sunday-1.2705834; http://earthobservatory.nasa.gov/IOTD/view.php?id=84042

Long et al. 2013), unusually large and intense wildfires and air pollution (Wendler et al. 2011; Shaposhnikov et al. 2014), die-offs of plants and animals (Bréda et al. 2006; McKechnie et al. 2012; Allen et al. 2015), the spread of infections (Baker-Austin et al. 2016), and loss of human life (Bouchama 2004; Sun et al. 2014; Fouillet et al. 2008; Elliot et al. 2014).

Comparison of verified heat waves with the Palmer drought severity index (PDSI) reveals close spatial association between positive LSTmax anomalies and drought stress and between negative LSTmax anomalies and moisture (Fig. 6). In 2007, heat waves affected western and southern/eastern North America (Fig. 6a). A cool summer anomaly occurred between the heat waves, resulting in negative (cool) and positive (hot) anomalies adjacent to one another. Displaying a similar general pattern, the PDSI for July of 2007 shows extreme, severe, and moderate drought impacts in the western and southern/eastern portions of the United States, with extremely moist conditions in Texas extending up into portions of the Midwest (Fig. 6b). In 2011, a large and intense positive LSTmax anomaly corresponded to the heat wave in Texas and Oklahoma and extended along the coast of the southeastern United States (Fig. 6c). The western United States experienced negative anomalies. The PDSI for July of 2011 shows similar spatial patterns with extreme and severe drought concentrated over Texas and Oklahoma and extending along the coast of the southeastern United States while moist conditions prevailed in the west (Fig. 6d). Note that smaller LSTmax anomaly patches in the northeastern United States during 2011 do not correspond to drought, indicating that not every LSTmax anomaly patch is indicative of a drought or heat wave. The large-scale

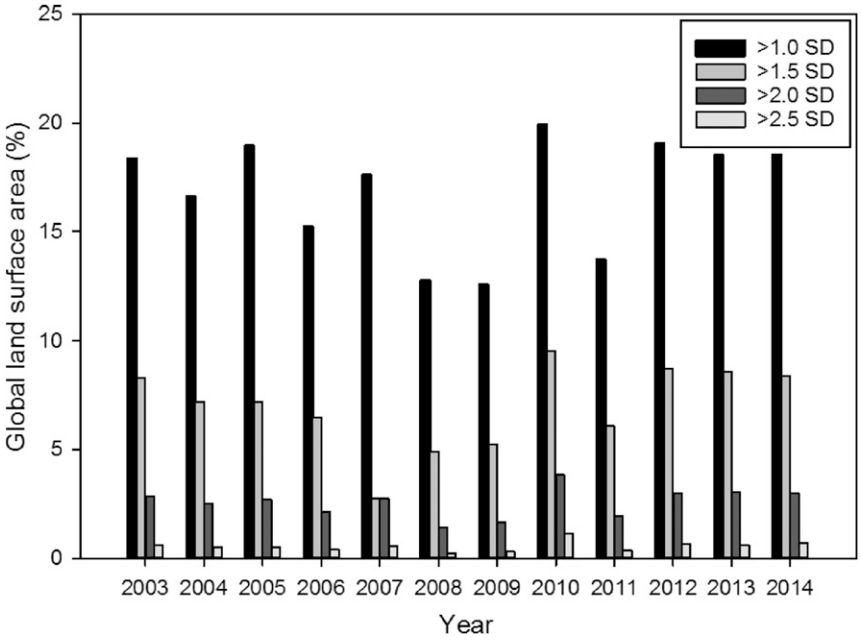

FIG. 4. Area affected by positive LSTmax standardized anomalies.

patterns do provide compelling evidence for the interaction between LSTmax anomalies and drought indices. Low maximum temperature anomalies generally imply cooler summer conditions that are less notable from a meteorological point of view, but we found these negative anomalies to be associated with verified climatic events, such as the cool summers of 2004 and 2009 in much of the central portion of the United States, the cool spring and summer of 2007 in Texas (Fig. 6a), and Australia's wet, cool summer in 2011.

Recent extreme heat events, such as those shown in Figs. 5 and 6, are redrawing the temperature records of the planet, breaking records from daily to seasonal time scales (Barriopedro et al. 2011; Lewis and Karoly 2013). To visualize the footprint of increasingly extreme heat waves on the planet's highest temperatures, we extracted the year during which the highest LSTmax occurred from 2003 to 2014 across the global land surface. The resulting map shows the temporal juxtaposition of large, severe heat waves, particularly in the Northern Hemisphere, such as the 2003 European heat wave (light pink) and the 2010 Siberian heat wave (light green) superimposed on other major heat waves from 2006 and 2012 (Fig. 7). The 2012 melt event in Greenland dominated the highest LSTmax over large areas of the ice sheet. North America shows the footprint of

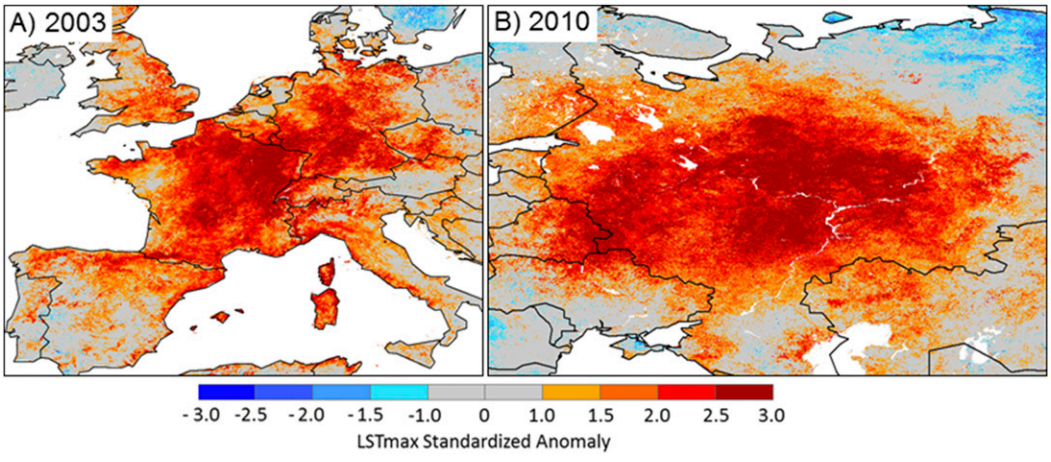

FIG. 5. Heat waves and LSTmax anomalies for (a) 2003 European and (b) 2010 Siberian heat waves.

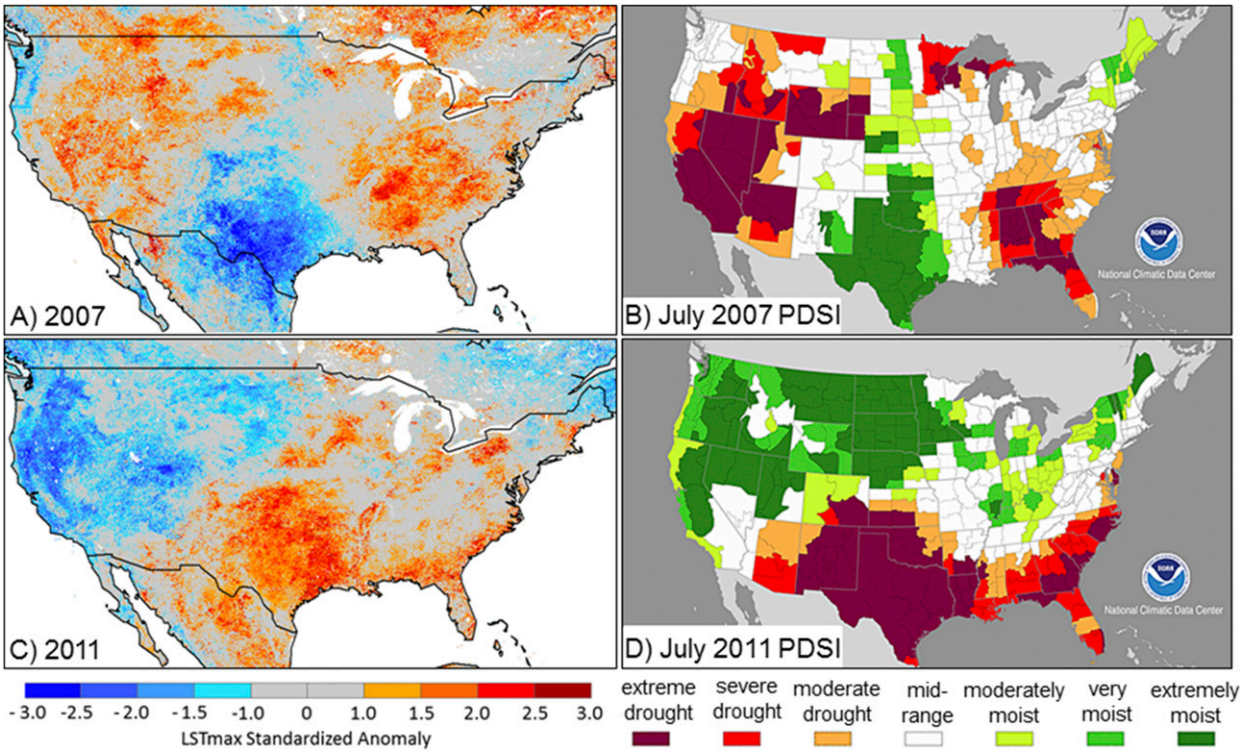

FIG. 6. LSTmax anomalies across the United States for (a) 2007 and (c) 2011 in comparison with the PDSI for (b) July 2007 and (d) July 2011.

numerous extreme events such as the 2003 heat wave in western North America, and the 2004 heat wave in southeastern Alaska (Fig. 7). The highest LSTmax values in the central and southeastern United States occurred during the heat waves in 2006, 2011, and 2012. In Australia, record-breaking heat waves in 2009 and 2013 dominate the timing of the highest LSTmax over large areas of the continent. The 2005 drought had a strong footprint in Africa. In South America, the 2009 heat wave in La Plata basin (green) and the 2013 heat wave in Argentina (orange) dominated the timing of the highest LSTmax in those areas. Patterns in tropical rain forests are generally more mixed, but the 2010 heat wave marked the dominant year during our study period for highest LSTmax in these forests.

b. *Cryosphere melt*

To isolate Earth's year-round ice- and snow-covered lands for melt detection, we extracted the 1-km^2 LSTmax data from 2003 to 2014 for all pixels classified as ice/snow by the MODIS Land Cover map of 2003. The global ice/snow LSTmax histogram accounts entirely for the low-temperature mode in the global histogram (Fig. 2), including the sharp spike at 0°C (32°F), the melting point of ice (Fig. 8). During the melt phase-change process, considerable energy is spent in the physical process of breaking hydrogen bonds rather than in increasing the surface temperature, resulting in a convergence of surface temperatures around the ice-melt temperature range. Close examination of the melting-point peak reveals large shifts between years (2011–14 shown in the Fig. 8 inset graph). In 2012 the peak reached its highest level, representing about 32 000 km^2 of the ice- and snow-covered land surface, higher than any other year by over 10 000 km^2. Interesting is that, once melt occurs, surface temperatures warm rapidly, as indicated by the relatively tiny fraction of Earth's surface with LSTmax between 0° and 10°C (Figs. 2 and 8). This suggests that the phase change acts as a climatic buffer that, once overcome, results in a rapid surface temperature increase.

To examine the location of ice melt, we mapped the temperature range associated with the ice-melt peak (approximately from −1.0° to 0.5°C) for four consecutive years (2011–14) and compared Greenland and Antarctica, which together contain 99% of the freshwater ice on Earth. The maps show ice melt concentrated in the Northern Hemisphere and especially on the GrIS, where large areas around the coastal margin display LSTmax values within the ice-melt range each year (Fig. 9). The increased surface melt during 2012 is clearly visible, indicating that the observed shift in the 2012 LSTmax histogram is tracking major melt changes in the cryosphere. In comparison,

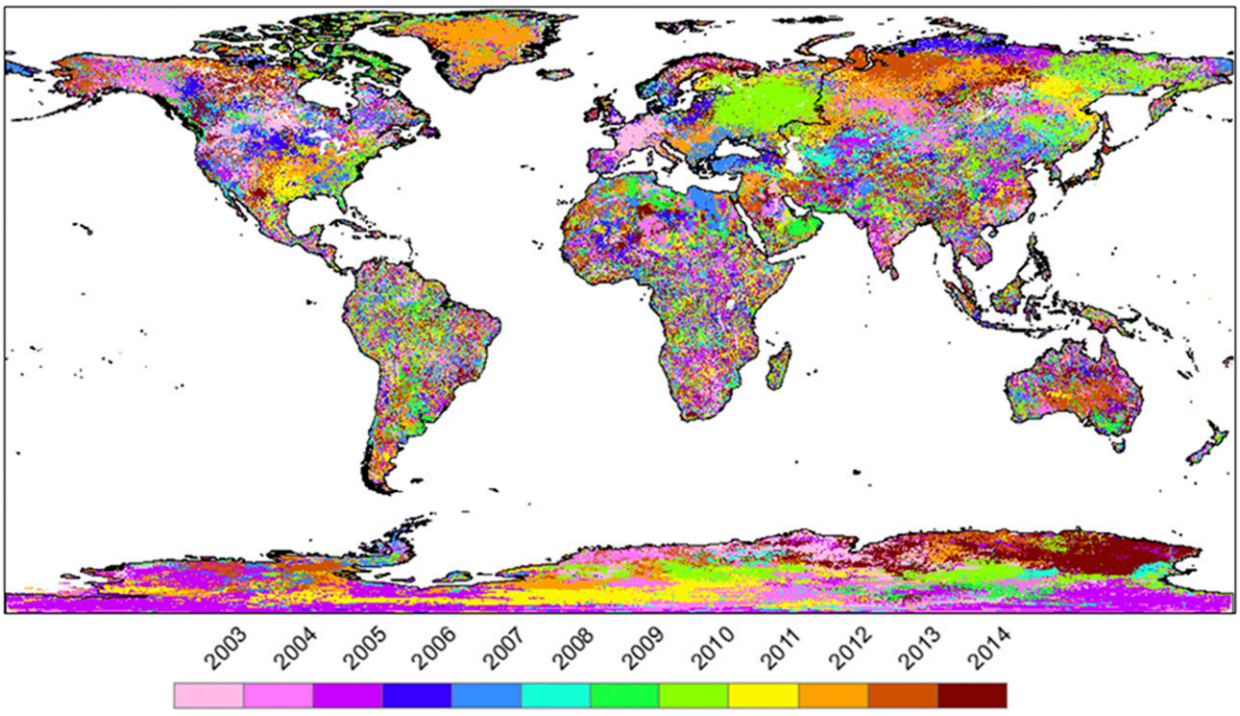

FIG. 7. The year during which the highest LSTmax occurred from 2003 to 2014 at every 1-km^2 pixel across the global land surface shows the temporal footprint of numerous large-scale heat waves.

Antarctica's LSTmax stayed mostly below the ice-melt range (Fig. 9).

The LSTmax histogram plotted specifically for Greenland verifies that melt on the GrIS drove the observed shifts in the global ice-/snowmelt peak, including the 2012 maximum that corresponds to the year of record melt and a widespread positive LSTmax anomaly (Fig. 10). Spatial patterns reveal that the 2012 LSTmax positive

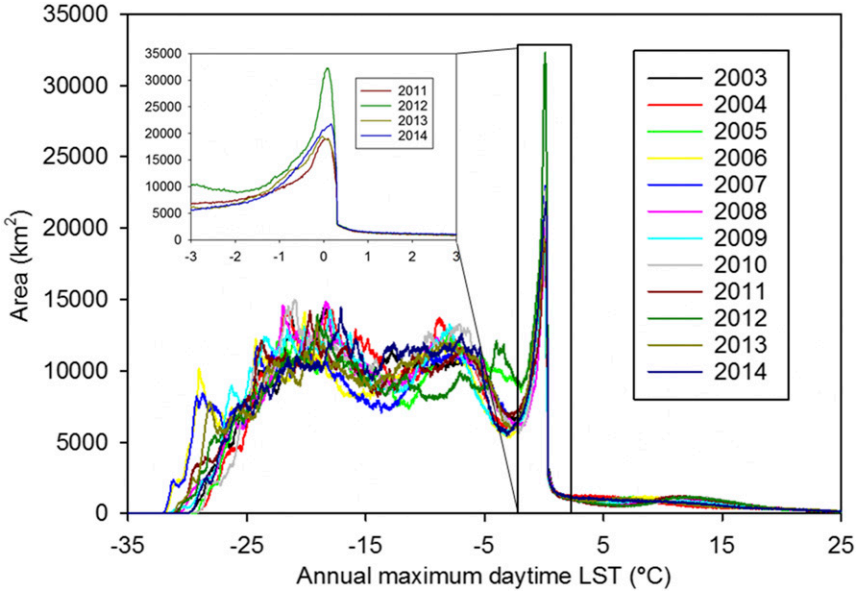

FIG. 8. The LSTmax histogram for all pixels labeled as ice/snow by MODIS Land Cover (2003) illustrates the unique and critical role of ice- and snow-covered lands in regulating the expression of Earth's upper temperature limit and reveals a strong kurtosis at the melting point with large interannual variability (inset graph).

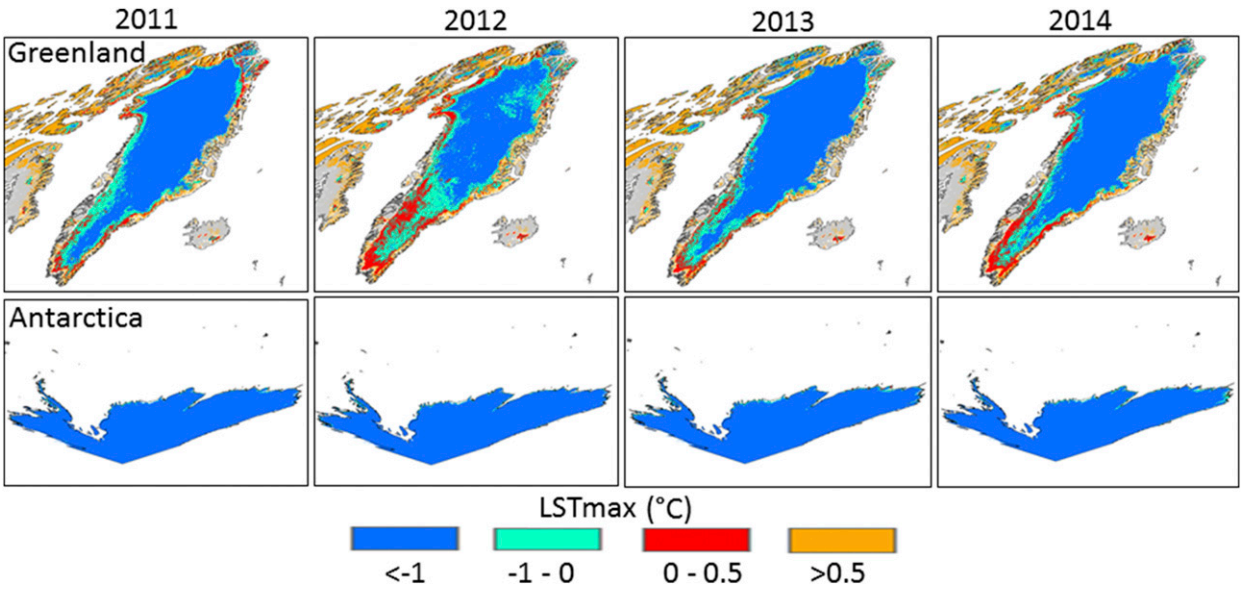

FIG. 9. Spatial location of ice/snow pixels with temperatures below (<−1°C), within (from −1° to 0.5°C) and above (>0.5°C) the ice-melt temperature range for (top) Greenland and (bottom) Antarctica. Note that the ice surface temperature of −1°C is used as a detection threshold for melt (Nghiem et al. 2012).

anomalies were most intense (>2.5 SD) in the northern interior part of the GrIS (Fig. 10a), which includes the cold polar areas at high altitudes where historical melt has been very rare (Clausen et al. 1988; Nghiem et al. 2012). In 2012 the pronounced positive anomalies resulted in surface temperatures that crossed the melt point in the cold polar areas. Also of importance is the shift toward warmer temperatures in 2012 for the entire LSTmax distribution of the GrIS relative to the other years, with the coldest temperatures rising to approximately −10°C, and a substantial increase in area of ice within the temperature range from −5° to 0°C (Fig. 10b). In comparison, much of Antarctica's ice/snow environment maintained cooler annual maximum surface temperatures, in the range from −30° to −5°C, and a much smaller peak at the melt point.

c. *Tropical-forest droughts*

To investigate the effects of major verified droughts on tropical forests, we isolated the LSTmax data for all

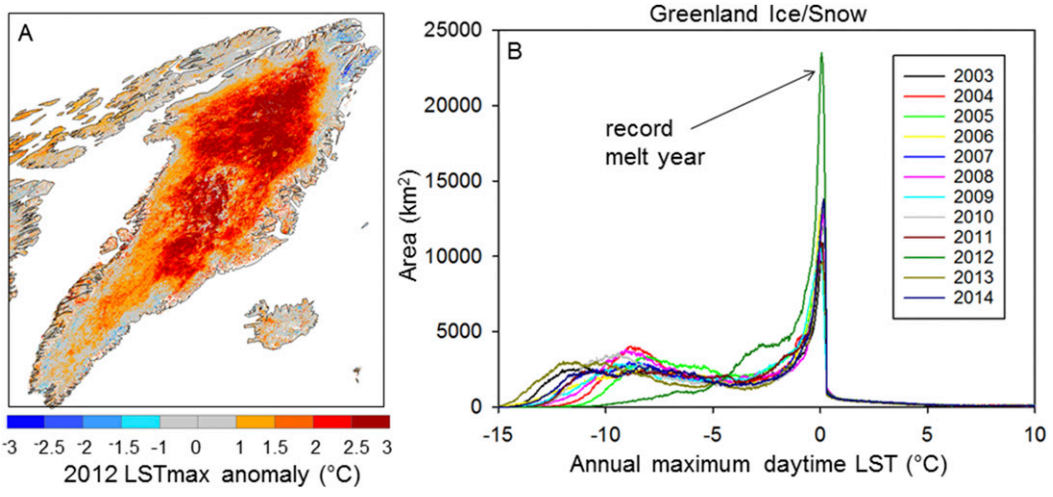

FIG. 10. (a) Spatial patterns of 2012 LSTmax positive anomalies extend across Greenland and are most intense in the northern interior of the ice sheet, which includes cold polar areas at high altitudes. (b) The entire distribution for Greenland shifted toward higher temperatures in 2012, with a substantial increase in the melting-point kurtosis.

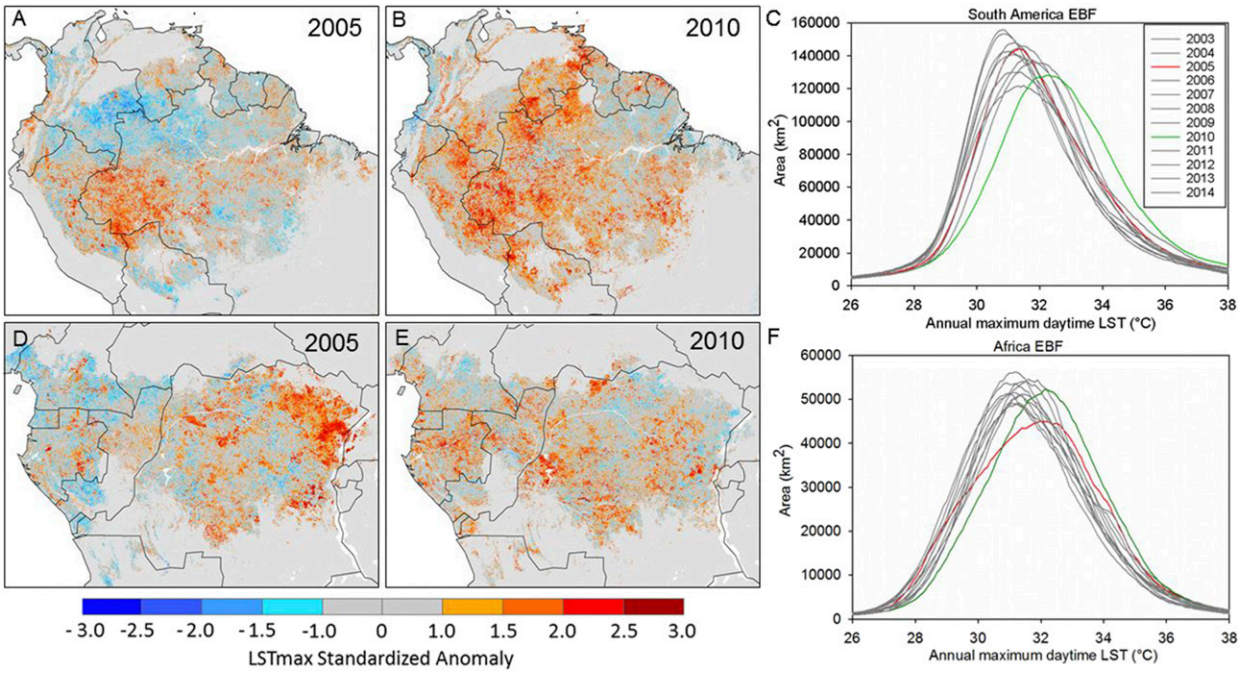

FIG. 11. Spatial patterns of LSTmax anomalies in the EBF during the droughts of (a),(d) 2005 and (b),(e) 2010 for the (top) Amazon and (bottom) Congo rain forests. Note that all non-EBF cover types are mapped in light gray. Also shown are the LSTmax histograms for all EBF pixels in (c) South America and (f) Africa, with all years in gray except for 2005 (red) and 2010 (green).

EBFs globally using the 2003 MODIS Land Cover dataset. These tropical forests account for a portion of the central mode in the global LSTmax histogram and consistently regulate LSTmax approximately between 25° and 35°C (Fig. 2). Amazonia experienced a widespread and severe drought in 2010 (Marengo et al. 2011). Severe drought also affected the Amazon rain forest in 2005 (Marengo et al. 2008). These recent Amazonian droughts are well documented, but in situ observations of drought effects are more limited in the central African rain forests. Recent studies have presented observational evidence for a widespread decline in vegetation greenness in Congolese forests in the past decade (Zhou et al. 2014). With our spatially continuous data we examined the LSTmax anomalies and distributions for South America (Amazon rain forest) and Africa (Congo rain forest), which contain the two largest rain forests on Earth.

We found that positive LSTmax anomalies affected both the Amazon and Congo rain forests during the major droughts of 2005 and 2010 (Fig. 11). In the Amazon in 2005, positive anomalies exceeded 1.5 SD and smaller patches that exceeded 2.0 SD were concentrated in the southwestern region (Fig. 11a), where patterns of drought impact on the forest canopy were most severe (Saatchi et al. 2013). In 2010 the positive LSTmax anomalies were much more widespread throughout the Amazon, with larger, high-severity patches in excess of 2.0 and 2.5 SD (Fig. 11b). These anomalous features drove a notable bulk shift toward higher temperatures in the 2010 LSTmax histogram for South America's EBF (Fig. 11c). The Congolese rain forests experienced intense positive anomalies during 2005 (>2.0 SD), especially in their central/eastern extent (Fig. 11d). The 2010 positive anomalies in the Congo were widespread across the forest, with scattered high-severity patches in excess of 2.0 SD (Fig. 11e). Of interest is that the LSTmax anomalies drove notable directional shifts toward higher temperatures in Africa's EBF in 2005 and 2010 (Fig. 11f).

d. Tropical-forest loss

It is well established that forest loss increases the LSTmax in tropical forests (Mildrexler et al. 2011a; Li et al. 2015). Thus, the cumulative effect of deforestation on LSTmax over time should shift the histograms toward higher temperatures. We found a shift toward higher LSTmax values between the first (2003–08) and second (2009–14) halves of the study period for all EBFs globally and for the EBF in South America (Figs. 12a,b). In the Amazon, the area of forest loss between 2002 and 2012 was largely concentrated in the "arc of deforestation" along the southern edge of the Amazon forest (Fig. 12c). The significant mean temperature changes (>2.5°C) showed strong spatial association with areas of forest loss and were nearly uniform toward higher temperatures (Fig. 12d).

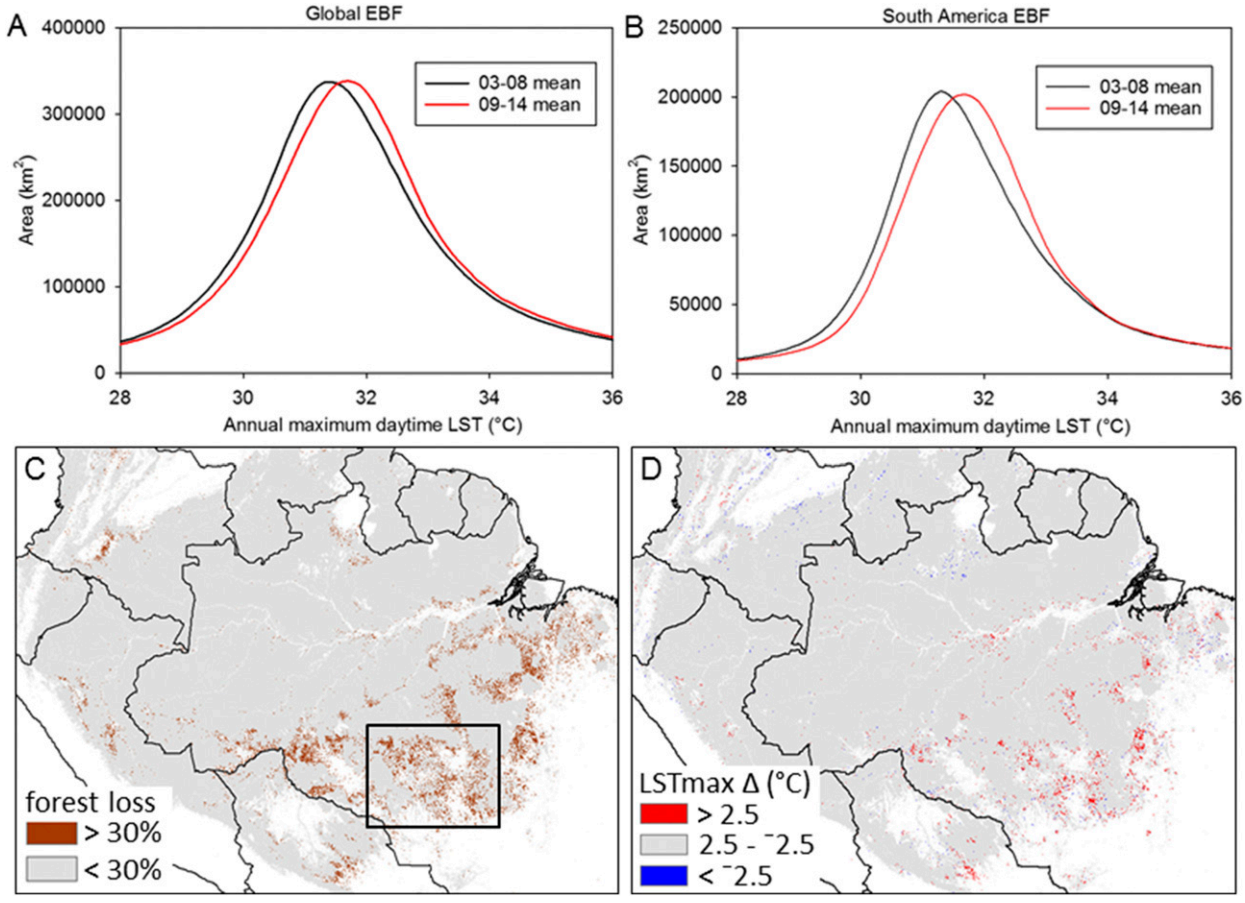

FIG. 12. The LSTmax histogram shifts between the first half (2003–08) and the second half (2009–14) of the study period for (a) all EBFs globally and (b) South America. Also shown are spatial patterns of (c) pixels with greater than 30% forest loss in Amazon EBF and (d) pixels that experienced significant mean temperature change between the first half (2003–08) and the second half (2009–14) of the study period.

We also isolated the area of EBF that experienced greater than 30% forest loss during our study period and plotted the temperature change against the area that experienced less than 30% forest loss. The area of 30% or more forest loss displayed a much larger shift toward higher temperatures than the area that experienced less than 30% forest loss (Figs. 13a,b). A typical area of forest loss in the Amazon reveals the tight spatial coupling between forest loss and LSTmax increases of more than 5°C between 2003 and 2014 at the local scale (Fig. 13c). Zooming in closer reveals the LSTmax changes in areas of visible forest loss (Fig. 13d). As compared with the area of increased temperature, very little area shows a reduction in LSTmax that would indicate recovery from previous forest loss.

4. Summary and discussion

The MODIS LSTmax anomalies capture detailed spatial patterns that are associated with droughts and heat waves across the global land surface (Fig. 3; Table 1). Because the LSTmax is the highest of the 8-day average values during an annual period, LSTmax provides important information on ecosystem exposure patterns to extreme temperatures. Rather than representing an instant in time when temperatures peaked, LSTmax captures a temporal period over which significant ecological effects can occur. This attribute improves the ability of LSTmax anomalies to detect the footprint of large-scale multiday heat waves and droughts that cause significant effects to ecosystems and to society (Figs. 5 and 6). Short-term heat waves of 1 or 2 days in duration should also be captured by the LSTmax anomalies because they will likely result in the highest annual LSTs of any 8-day period, but it is also possible that the intensity of shorter-term events could be muted by the 8-day composite period.

The close proximity of warm and cool anomalies emerged as an important spatial pattern highlighting how LST can change rapidly over short distances.

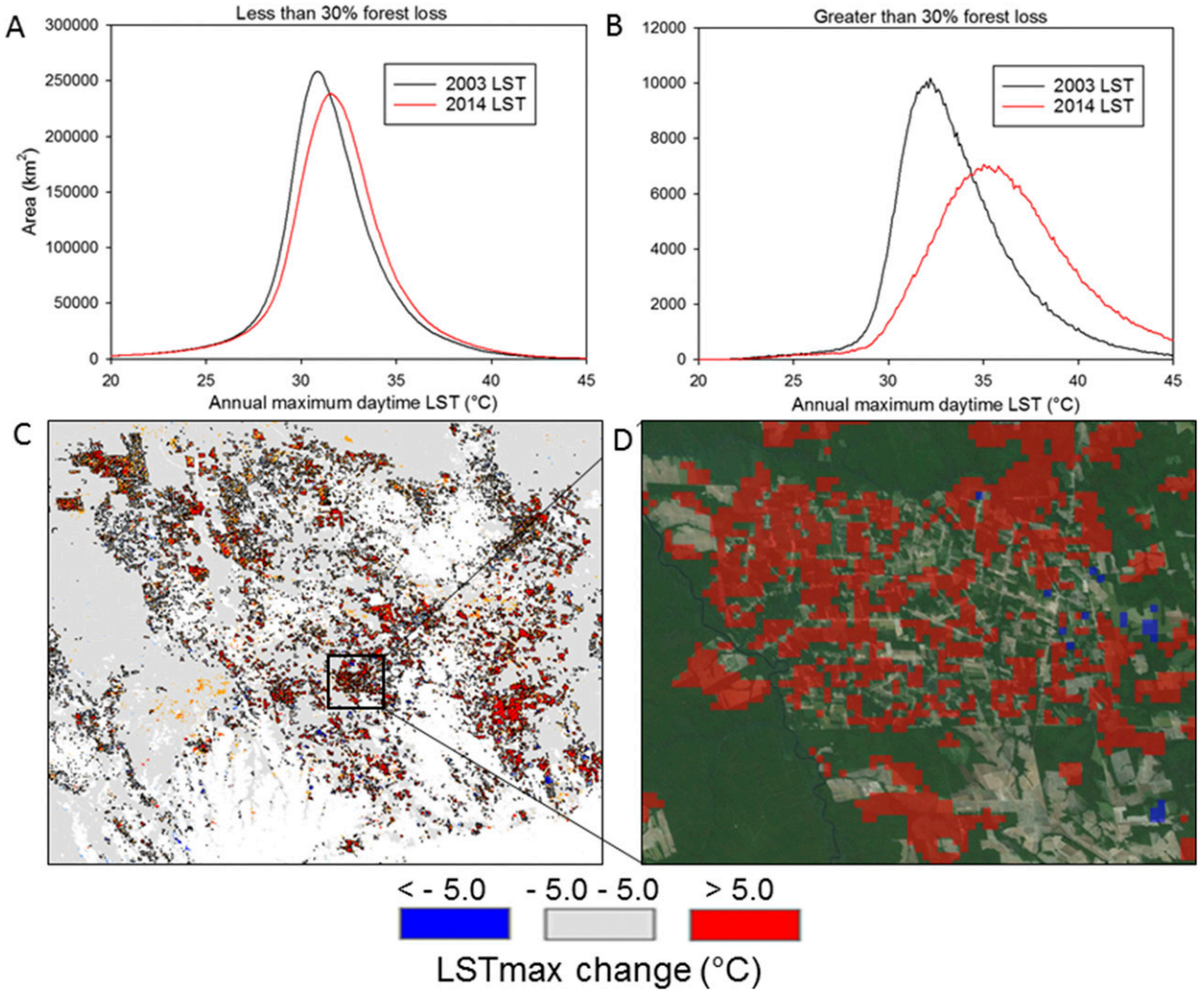

FIG. 13. The 2003 and 2014 LSTmax histograms for EBF, comparing (a) the area with less than 30% forest loss with (b) the area with more than 30% forest loss. Also shown is (c) the spatial association between temperature changes and 30% forest loss polygons (mapped in black crosshatching) in the Amazon (the location corresponds to the box in Fig. 12c). (d) A zoomed-in view showing in more detail the association between temperature changes and visible signs of forest loss (image source: Esri, DigitalGlobe, GeoEye, i-cubed, USDA, USGS, AEX, Getmapping, Aerogrid, IGN, IGP, swisstopo, and the GIS User Community).

Moreover, the close spatial association between positive LSTmax anomalies and drought severity and between negative LSTmax anomalies and moisture from the PDSI provides compelling evidence for the highly contrasting ecological conditions in these areas (Fig. 6). The 1-km resolution of the LSTmax data provides much greater spatial detail to analyze how these contrasting temperatures express over the land surface. This information is critical for improved quantification of ecosystem exposure patterns to extreme temperatures.

Our results document that Earth's maximum surface temperatures are experiencing biome-scale bulk shifts toward anomalously high temperatures in association with large-scale extreme climatic events and land-use change. Large-scale directional shifts in maximum temperatures indicate important changes in the surface energy balance that push ecosystems and biomes toward critical thresholds. We found these shifts in the cryosphere in conjunction with the extreme melt of the GrIS and in tropical rain forests as a result of widespread and severe drought and the cumulative effects of forest loss. Biome-level bulk shifts in the LSTmax distribution indicate the potential for thermal stress thresholds to be crossed for large areas, resulting in profound and irreversible changes. For example, 98.6% of the GrIS was under melt in 2012 (Nghiem et al. 2012) in conjunction with widespread positive LSTmax anomalies and a large increase in the ice-melt peak of Greenland's histogram (Fig. 10). Melt occurred in the high polar altitudes of the GrIS in some areas where the last significant melt event

is recorded in the 1889 ice layer (Clausen et al. 1988). Ice loss from the GrIS has rapidly accelerated during the last four years of our study period (2011–14) accounting for an increasing proportion of global sea level rise, and the greatest ice loss occurred during the exceptionally warm summer of 2012 (McMillan et al. 2016). The 2012 LSTmax anomalies indicate that in future extreme melt years the most intense anomalies will manifest in the high-altitude polar areas of the ice sheet, shifting the GrIS LSTmax summer histogram distribution. These results provide a glimpse into how future summer temperature distributions will look under a melt regime characterized by a 100% summer surface ice-melt extent, a threshold-reaching condition that will likely trigger tipping points in the ice-sheet melt regime (Box et al. 2012). The unique phase-change-driven component to the ice/snow histogram will also provide valuable insights into future ice-melt changes in Antarctica.

In a result that demonstrates the importance of wall-to-wall global LST coverage, we found that the Amazon and Congo rain forests experienced widespread LSTmax anomalies and large-scale directional shifts toward higher temperatures in 2010 and, to a lesser extent, in 2005. The 2010 LSTmax anomalies show how large, severe droughts, such as occurred in 2010 (Marengo et al. 2011), can rapidly shift an entire forest biome toward a condition of increased thermal stress (Fig. 11). Given that the 2010 drought caused a widespread reduction in vegetation greenness, increased mortality, and reduced growth that may have shut down the entire Amazon rain-forest carbon sink (Lewis et al. 2011; Xu et al. 2011; Feldpausch et al. 2016), the effects of the 2005 and 2010 LSTmax anomalies on the Congolese forests were most likely also severe. This likelihood is consistent with the gradual decline in photosynthetic capacity and moisture content that was observed in the Congolese forests over a similar time period (Zhou et al. 2014). It is not surprising that, in comparison with 2005, the 2010 drought had a much stronger effect on shifting the LSTmax distribution in the Amazon rain forest. Although both Amazonian droughts were severe, the 2010 drought caused declines in greenness that spanned an area that was nearly 5 times as large as that of 2005 (Xu et al. 2011). Research into the effects of recent subcontinental hotter droughts on tree mortality have found that consecutive multiyear events cause progressive drying of the forest canopy and reductions in soil moisture that can result in widespread mortality of dominant trees species (Breshears et al. 2005; Asner et al. 2016). Extreme drought events have legacy effects on forest ecosystems that can last for several years, potentially reducing the resiliency of ecosystems to subsequent drought events (Bréda et al. 2006; Anderegg et al. 2015; Saatchi et al. 2013). As the area affected by extreme high temperatures increases (Hansen et al. 2012), so will the exposure of ecosystems to anomalously high temperatures, reducing recovery time and pushing ecosystems closer to resilience limits across large scales. Since the temporal responses in energy exchanges to heat waves and droughts can vary between land-cover types with commensurate effects on the expression of daytime maximum temperatures (Teuling et al. 2010), LSTmax coupled with land-cover-type information can provide a high level of discernment of how multiyear droughts progress across diverse landscapes that is not possible with some traditional drought metrics (Figs. 5 and 6).

Forest cover changes are a key driver of anthropogenic climate change (Bonan 2008). Thus, the ability to detect human-induced forest loss is a critical aspect of the LSTmax global indicator. The shift in the mean LSTmax toward higher temperatures between the first half and the second half of our study period demonstrates how the temperature effects of annual forest-cover changes accrue over time (Fig. 12). The changes detected here are from a 2003 land-cover baseline, but by 2003 more than 837 000 km^2 of Amazonian forests had already been lost (Malhi et al. 2008). Given the increases in LSTmax we detected from 2003 to 2014 in association with forest loss (Fig. 13) and the well-documented increases in maximum temperature resulting from tropical-forest loss (Nemani et al. 1996; Mildrexler et al. 2011a; Li et al. 2015, 2016), historic forest loss has driven even more widespread increases in LSTmax with commensurate impacts on regional climate. Together, the effects of forest loss and climate change amplify one another, and our analysis provides a new integrated way to examine these critical changes.

This study has shown the immense value of a single, unique measurement in tracking critical changes in the Earth system. The focus on changing thermal regimes has the potential to detect the shifts of ecosystems toward thresholds of profound change and our global, semiautomated annual analysis is easily repeatable for continuous monitoring of the entire land surface of Earth. These are important distinctions from disturbance-detection approaches that employ complex algorithms to provide detailed information on abrupt disturbances and land-cover change but are rarely applied annually over the entire land surface of Earth. As part of a global disturbance-monitoring system, our efficient global analysis could identify areas for further examination with higher-spatial-resolution imagery such as the 30-m Landsat product (McDowell et al. 2015). Given the link between warming temperatures and increasing rates of disturbance (Allen et al. 2015),

we contend that the focus of our method on bulk shifts in surface temperatures provides a more informative first-look global-change indicator when compared with coarse-scale disturbance detection information alone.

A 12-yr period is insufficient to attribute the LSTmax changes to anthropogenic climate change or to establish long-term trends. Nonetheless, our results show that large-scale heat waves and droughts can rapidly change the LSTmax spatial patterns, resulting in increased melt in the cryosphere and widespread drought stress in tropical forests. It is important to note that the LSTmax metric is detecting major biospheric change and not directional climate change. However, climate change provides context for understanding the extreme events that are occurring more frequently (Seneviratne et al. 2014; Perkins et al. 2012; Hansen et al. 2012). Over time, extreme temperature events, especially heat waves and droughts, play an important role in redefining Earth's surface thermal maxima (Fig. 7) and ultimately the global LSTmax histograms. As more years of data accumulate, trends in LSTmax could be examined. We conclude that with continued climate warming, Earth's integrated maximum temperatures will likely experience greater and more frequent directional shifts. This will increase the likelihood that critical thresholds will be surpassed, resulting in regional-scale transitions that are tipping points in the global climate system (Chapin et al. 2008; Hilker et al. 2014). Given the unique qualities of the LSTmax measurement and the importance of continuing this annual analysis for future trend detection, data continuity in satellite-derived LST is imperative. Subsequent research will investigate the ability of the LSTmax indicator to detect slower biome shifts such as changes in woody plant cover in the Arctic that are altering the surface energy balance and the ongoing land degradation in the Sahel of Africa.

Acknowledgments. This study was supported by the U.S. Department of Agriculture Forest Service Pacific Northwest Research Station and Oregon State University. Author DM designed the study with the help of authors MZ and SR. Author DM analyzed data, interpreted results, and wrote the manuscript, with authors MZ and WC helping with the writing. Authors MZ and XS processed data. All authors contributed to interpreting the results and refining the manuscript. The authors declare that they have no competing interests. All data needed to evaluate the conclusions in the paper are present in the paper. Additional data related to this paper may be requested from the authors. MODIS data used in this work are available from the Land Processes Distributed Active Archive Center (https://lpdaac.usgs.gov/dataset_discovery/modis/modis_products_table).

REFERENCES

Allen, C. D., D. D. Breshears, and N. G. McDowell, 2015: On underestimation of global vulnerability to tree mortality and forest die-off from hotter drought in the Anthropocene. *Ecosphere*, **6**, 129, https://doi.org/10.1890/ES15-00203.1.

Anderegg, W. R. L., and Coauthors, 2015: Pervasive drought legacies in forest ecosystems and their implications for carbon cycle models. *Science*, **349**, 528–532, https://doi.org/10.1126/science.aab1833.

Asner, G. P., P. G. Brodick, C. B. Anderson, N. Vaughn, D. E. Knapp, and R. E. Martin, 2016: Progressive forest canopy water loss during the 2012–2015. *Proc. Natl. Acad. Sci. USA*, **113**, E249–E255, https://doi.org/10.1073/pnas.1523397113.

Baker-Austin, C., J. A. Trinanes, S. Salmenlinna, M. Löfdahl, A. Siitonen, N. G. H. Taylor, and J. Martinez-Urtaza, 2016: Heat wave–associated vibriosis, Sweden and Finland, 2014. *Emerg. Infect. Dis.*, **22**, 1216–1220, https://doi.org/10.3201/eid2207.151996.

Barriopedro, D., E. M. Fischer, J. Luterbacher, R. M. Trigo, and R. Garcia-Herrera, 2011: The hot summer of 2011: Redrawing the temperature record map of Europe. *Science*, **332**, 220–224, https://doi.org/10.1126/science.1201224.

Bateni, S. M., and D. Entekhabi, 2012: Relative efficiency of land surface energy balance components. *Water Resour. Res.*, **48**, W04510, https://doi.org/10.1029/2011WR011357.

Bonan, G. B., 2008: Forests and climate change: Forcings, feedbacks, and the climate benefits of forests. *Science*, **320**, 1444–1449, https://doi.org/10.1126/science.1155121.

Bouchama, A., 2004: The 2003 European heat wave. *Intensive Care Med.*, **30**, 1–3, https://doi.org/10.1007/s00134-003-2062-y.

Bowman, D. M. J. S., J. K. Balch, P. Artaxo, W. J. Bond, J. M. Carlson, and M. A. Cochrane, 2009: Fire in the earth system. *Science*, **324**, 481–484, https://doi.org/10.1126/science.1163886.

Box, J. E., X. Fettweis, J. C. Stroeve, M. Tedesco, D. K. Hall, and K. Steffen, 2012: Greenland ice sheet albedo feedback: Thermodynamics and atmospheric drivers. *Cryosphere*, **6**, 821–839, https://doi.org/10.5194/tc-6-821-2012.

Bréda, N., R. Huc, A. Granier, and E. Dreyer, 2006: Temperate forest trees and stands under severe drought: A review of ecophysiological responses, adaptation processes and long-term consequences. *Ann. For. Sci.*, **63**, 625–644, https://doi.org/10.1051/forest:2006042.

Breshears, D. D., and Coauthors, 2005: Regional vegetation die-off in response to global-change type drought. *Proc. Natl. Acad. Sci.*, **102**, 15 144–15 148, https://doi.org/10.1073/pnas.0505734102.

Bromwich, D. H., J. P. Nicolas, A. J. Monaghan, M. A. Lazzara, L. M. Keller, G. A. Weidner, and A. B. Wilson, 2013: Central West Antarctica among the most rapidly warming regions on Earth. *Nat. Geosci.*, **6**, 139–145, https://doi.org/10.1038/ngeo1671.

Bumbaco, K. A., and P. W. Mote, 2010: Three recent flavors of drought in the Pacific Northwest. *J. Appl. Meteor. Climatol.*, **49**, 2058–2068, https://doi.org/10.1175/2010JAMC2423.1.

Bustinza, R., G. Lebel, P. Gosselin, D. Belanger, and F. Chebana, 2013: Health impacts of the July 2010 heat wave in Québec, Canada. *BMC Public Health*, **13**, 56, https://doi.org/10.1186/1471-2458-13-56.

Cai, S., D. Liu, D. Sulla-Menashe, and M. A. Friedl, 2014: Enhancing MODIS land cover product with a spatial–temporal modeling algorithm. *Remote Sens. Environ.*, **147**, 243–255, https://doi.org/10.1016/j.rse.2014.03.012.

Cattiaux, J., and P. Yiou, 2013: U.S. heat waves of spring and summer 2012 from the flow-analogue perspective [in "Explaining Extreme Events of 2012 from a Climate Perspective"]. *Bull. Amer. Meteor. Soc.*, **94** (9), S10–S13, https://doi.org/10.1175/BAMS-D-13-00085.1.

Chapin, F. S., III, J. T. Randerson, A. D. McGuire, J. A. Foley, and C. B. Field, 2008: Changing feedbacks in the climate–biosphere system. *Front. Ecol. Environ.*, **6**, 313–320, https://doi.org/10.1890/080005.

Chen, J. L., C. R. Wilson, B. D. Tapley, L. Longuevergne, Z. L. Yang, and B. R. Scanlon, 2010: Recent La Plata basin drought conditions observed by satellite gravimetry. *J. Geophys. Res.*, **115**, D22108, https://doi.org/10.1029/2010JD014689.

Christidis, N., G. S. Jones, and P. A. Stott, 2015: Dramatically increasing chance of extremely hot summers since the 2003 European heatwave. *Nat. Climate Change*, **5**, 46–50, https://doi.org/10.1038/nclimate2468.

Ciais, P., and Coauthors, 2005: Europe-wide reduction in primary productivity caused by the heat and drought in 2003. *Nature*, **437**, 529–533, https://doi.org/10.1038/nature03972.

Clausen, H. B., N. S. Gundestrup, S. J. Johnsen, R. Bindschadler, and J. Zwally, 1988: Glaciological investigations in the Crete area, central Greenland: A search for a new deep-drilling site. *Ann. Glaciol.*, **10**, 10–15, https://doi.org/10.1017/S0260305500004080.

Cook, B. I., J. E. Smerdon, R. Seager, and S. Coats, 2014: Global warming and 21st century drying. *Climate Dyn.*, **43**, 2607–2627, https://doi.org/10.1007/s00382-014-2075-y.

Coops, N. C., D. C. Duro, M. A. Wulder, and T. Han, 2007: Estimating afternoon MODIS land surface temperatures (LST) based on morning MODIS overpass, location and elevation information. *Int. J. Remote Sens.*, **28**, 2391–2396, https://doi.org/10.1080/01431160701294653.

Coumou, D., and S. Rahmstorf, 2012: A decade of weather extremes. *Nat. Climate Change*, **2**, 491–496, https://doi.org/10.1038/nclimate1452.

Cox, P. M., R. A. Betts, M. Collins, P. P. Harris, C. Huntingford, and C. D. Jones, 2004: Amazonian forest dieback under climate–carbon cycle projections for the 21st century. *Theor. Appl. Climatol.*, **78**, 137–156, https://doi.org/10.1007/s00704-004-0049-4.

Daly, C., M. Halbleib, J. I. Smith, W. P. Gibson, M. K. Doggett, G. H. Taylor, J. Curtis, and P. P. Pasteris, 2008: Physiographically-sensitive mapping of temperature and precipitation across the conterminous United States. *Int. J. Climatol.*, **28**, 2031–2064, https://doi.org/10.1002/joc.1688.

Elliot, A. J., and Coauthors, 2014: Using real-time syndromic surveillance to assess the health impacts of the 2013 heatwave in England. *Environ. Res.*, **135**, 31–36, https://doi.org/10.1016/j.envres.2014.08.031.

Feldpausch, T. R., and Coauthors, 2016: Amazon forest response to repeated droughts. *Global Biogeochem. Cycles*, **30**, 964–982, https://doi.org/10.1002/2015GB005133.

Fischer, E. M., and C. Schär, 2010: Consistent geographical patterns of changes in high-impact European heatwaves. *Nat. Geosci.*, **3**, 398–403, https://doi.org/10.1038/ngeo866.

Fouillet, A., and Coauthors, 2008: Has the impact of heat waves on mortality changed in France since the European heat wave of summer 2003? A study of the 2006 heat wave. *Int. J. Epidemiol.*, **37**, 309–317, https://doi.org/10.1093/ije/dym253.

Founda, D., and C. Giannakopoulos, 2009: The exceptionally hot summer of 2007 in Athens, Greece—A typical summer in the future climate? *Global Planet. Change*, **67**, 227–236, https://doi.org/10.1016/j.gloplacha.2009.03.013.

Friedl, M. A., and F. W. Davis, 1994: Sources of variation in radiometric surface temperature over a tallgrass prairie. *Remote Sens. Environ.*, **48**, 1–17, https://doi.org/10.1016/0034-4257(94)90109-0.

——, and Coauthors, 2002: Global land cover mapping from MODIS: Algorithms and early results. *Remote Sens. Environ.*, **83**, 287–302, https://doi.org/10.1016/S0034-4257(02)00078-0.

——, D. Sulla-Menashe, B. Tan, A. Schneider, N. Ramankutty, A. Sibley, and X. M. Huang, 2010: MODIS Collection 5 global land cover: Algorithm refinements and characterization of new datasets. *Remote Sens. Environ.*, **114**, 168–182, https://doi.org/10.1016/j.rse.2009.08.016.

Fuhrmann, C. M., C. E. Konrad II, M. M. Kovach, and D. J. Perkins, 2011: The August 2007 heat wave in North Carolina: Meteorological factors and local variability. *Phys. Geogr.*, **32**, 217–240, https://doi.org/10.2747/0272-3646.32.3.217.

Goward, S. N., G. D. Cruickshanks, and A. S. Hope, 1985: Observed relation between thermal emission and reflected spectral radiance of a complex vegetated landscape. *Remote Sens. Environ.*, **18**, 137–146, https://doi.org/10.1016/0034-4257(85)90044-6.

——, and Coauthors, 2008: Forest disturbance and North American carbon flux. *Eos, Trans. Amer. Geophys. Union*, **89**, 105–116, https://doi.org/10.1029/2008EO110001.

Grimm, N. B., and Coauthors, 2013: The impacts of climate change on ecosystem structure and function. *Front. Ecol. Environ.*, **11**, 474–482, https://doi.org/10.1890/120282.

Grumm, R. H., 2011: The central European and Russian heat event of July–August 2010. *Bull. Amer. Meteor. Soc.*, **92**, 1285–1296, https://doi.org/10.1175/2011BAMS3174.1.

——, and R. Hart, 2001: Standardized anomalies applied to significant cold season weather events: Preliminary findings. *Wea. Forecasting*, **16**, 736–754, https://doi.org/10.1175/1520-0434(2001)016<0736:SAATSC>2.0.CO;2.

Hansen, J., M. Sato, R. Ruedy, K. Lo, D. W. Lea, and M. Medina-Elizade, 2006: Global temperature change. *Proc. Natl. Acad. Sci. USA*, **103**, 14 288–14 293, https://doi.org/10.1073/pnas.0606291103.

——, ——, and ——, 2012: Perception of climate change. *Proc. Natl. Acad. Sci. USA*, **109**, E2415–E2423, https://doi.org/10.1073/pnas.1205276109.

Hansen, M. C., and Coauthors, 2013: High-resolution global maps of 21st-century forest cover change. *Science*, **342**, 850–853, https://doi.org/10.1126/science.1244693.

Hastenrath, S., D. Polzin, and C. Mutai, 2007: Diagnosing the 2005 drought in equatorial East Africa. *J. Climate*, **20**, 4628–4637, https://doi.org/10.1175/JCLI4238.1.

He, T., S. Liang, Y. Yu, Q. Liu, D. Wang, F. Gao, and Q. Liu, 2013: Greenland surface albedo changes in July 1981–2012 from satellite observations. *Environ. Res. Lett.*, **8**, 044043, https://doi.org/10.1088/1748-9326/8/4/044043.

Hilker, T., A. I. Lyapustin, C. J. Tucker, F. G. Hall, R. B. Myneni, Y. Wang, J. Bi, Y. Mendes de Moura, and P. J. Sellers, 2014: Vegetation dynamics and rainfall sensitivity of the Amazon. *Proc. Natl. Acad. Sci. USA*, **111**, 16 041–16 046, https://doi.org/10.1073/pnas.1404870111.

Hoerling, M., and Coauthors, 2013: Anatomy of an extreme event. *J. Climate*, **26**, 2811–2832, https://doi.org/10.1175/JCLI-D-12-00270.1.

Holmgren, M., and Coauthors, 2006: Extreme climatic events shape arid and semiarid ecosystems. *Front. Ecol. Environ.*, **4**, 87–95, https://doi.org/10.1890/1540-9295(2006)004[0087:ECESAA]2.0.CO;2.

IPCC, 2013: *Climate Change 2013: The Physical Science Basis*. Cambridge University Press, 1535 pp.

Janetos, A. C., R. S. Chen, D. Arndt, and M. A. Kenney, 2012: National Climate Assessment indicators: Background, development, and examples. U.S. Global Change Research Program National Climate Assessment Tech. Input Rep., 59 pp., https://doi.org/10.7916/D8RB7D2T.

Jentsch, A., J. Kreyling, and C. Beierkuhnlein, 2007: A new generation of climate change experiments: Events, not trends. *Front. Ecol. Environ.*, **5**, 365–374, https://doi.org/10.1890/1540-9295(2007)5[365:ANGOCE]2.0.CO;2.

Jin, M., and R. E. Dickinson, 2010: Land surface skin temperature climatology: Benefitting from the strengths of satellite observations. *Environ. Res. Lett.*, **5**, 044004, https://doi.org/10.1088/1748-9326/5/4/044004.

——, and T. J. Mullens, 2012: Land–biosphere–atmosphere interactions over the Tibetan plateau from MODIS observations. *Environ. Res. Lett.*, **7**, 014003, https://doi.org/10.1088/1748-9326/7/1/014003.

Karl, T. R., and Coauthors, 2012: U.S. temperature and drought: Recent anomalies and trends. *Eos, Trans. Amer. Geophys. Union*, **93**, 473–474, https://doi.org/10.1029/2012EO470001.

Karoly, D. J., 2009: The recent bushfires and extreme heat wave in southeast Australia. *Bull. Aust. Meteor. Oceanogr. Soc.*, **22**, 10–13, https://drive.google.com/drive/folders/0B_V-fcpNMrJjOTlPSi11dVdzMlk.

Kenney, M. A., and A. C. Janetos, 2014: National climate indicators system report. National Climate Assessment and Development Advisory Committee Tech. Rep., 157 pp., https://scholarworks.umt.edu/cgi/viewcontent.cgi?referer=http://scholar.google.com/&httpsredir=1&article=1375&context=ntsg_pubs.

Khan, S. A., and Coauthors, 2014: Sustained mass loss of the northeast Greenland ice sheet triggered by regional warming. *Nat. Climate Change*, **4**, 292–299, https://doi.org/10.1038/nclimate2161.

Knapp, A. K., and M. D. Smith, 2001: Variation among biomes in temporal dynamics of aboveground primary production. *Science*, **291**, 481–484, https://doi.org/10.1126/science.291.5503.481.

Kogan, F. N., 1997: Global drought watch from space. *Bull. Amer. Meteor. Soc.*, **78**, 621–636, https://doi.org/10.1175/1520-0477(1997)078<0621:GDWFS>2.0.CO;2.

Lambin, E. F., and D. Ehrlich, 1995: Combining vegetation indices and surface temperature for land-cover mapping at broad spatial scales. *Int. J. Remote Sens.*, **16**, 573–579, https://doi.org/10.1080/01431169508954423.

Lee, X., and Coauthors, 2011: Observed increase in local cooling effect of deforestation at higher latitudes. *Nature*, **479**, 384–387, https://doi.org/10.1038/nature10588.

Lenaerts, J. T. M., J. H. van Angelen, M. R. van den Broeke, A. S. Gardner, B. Wouters, and E. van Meijgaard, 2013: Irreversible mass loss of Canadian Arctic Archipelago glaciers. *Geophys. Res. Lett.*, **40**, 870–874, https://doi.org/10.1002/grl.50214.

Lewis, S. C., and D. J. Karoly, 2013: Anthropogenic contributions to Australia's record summer temperatures of 2013. *Geophys. Res. Lett.*, **40**, 3705–3709, https://doi.org/10.1002/grl.50673.

Lewis, S. L., P. M. Brando, O. L. Phillips, G. M. F. van der Heijden, and D. Nepstad, 2011: The 2010 Amazon drought. *Science*, **331**, 554, https://doi.org/10.1126/science.1200807.

Li, Y., M. Zhao, S. Motesharrei, Q. Mu, E. Kalnay, and S. Li, 2015: Local cooling and warming effects of forests based on satellite observations. *Nat. Commun.*, **6**, 6603, https://doi.org/10.1038/ncomms7603.

——, and Coauthors, 2016: Potential and actual impacts of deforestation and afforestation on land surface temperature. *J. Geophys. Res. Atmos.*, **121**, 14 372–14 386, https://doi.org/10.1002/2016JD024969.

Li, Z. L., B. H. Tang, H. Wu, H. Ren, G. Yan, Z. Wan, I. F. Trigo, and J. A. Sobrino, 2013: Satellite-derived land surface temperature: Current status and perspectives. *Remote Sens. Environ.*, **131**, 14–37, https://doi.org/10.1016/j.rse.2012.12.008.

Long, D., B. R. Scanlon, L. Longuevergne, A. Y. Sun, D. N. Fernando, and H. Save, 2013: GRACE satellites monitor large depletion in water storage in response to the 2011 drought in Texas. *Geophys. Res. Lett.*, **40**, 3395–3401, https://doi.org/10.1002/grl.50655.

Malhi, Y., J. T. Roberts, R. A. Betts, T. J. Killeen, W. H. Li, and C. A. Nobre, 2008: Climate change, deforestation, and the fate of the Amazon. *Science*, **319**, 169–172, https://doi.org/10.1126/science.1146961.

——, L. E. O. C. Aragão, D. Galbraith, C. Huntingford, R. Fisher, P. Zelazowski, S. Sitch, C. McSweeney, and P. Meir, 2009: Exploring the likelihood and mechanism of a climate-change-induced dieback of the Amazon rainforest. *Proc. Natl. Acad. Sci. USA*, **106**, 20 610–20 615, https://doi.org/10.1073/pnas.0804619106.

Mannstein, H., 1987: Surface energy budget, surface temperature and thermal inertia. *Remote Sensing Applications in Meteorology and Climatology*, R. A. Vaughan and D. Reidel, Eds., Reidel, 391–410.

Marengo, J. A., C. Nobre, J. Tomasella, G. Sampaio, and H. Camargo, 2008: The drought of Amazonia in 2005. *J. Climate*, **21**, 495–516, https://doi.org/10.1175/2007JCLI1600.1.

——, J. Tomasella, L. M. Alves, W. R. Soares, and D. A. Rodriguez, 2011: The drought of 2010 in the context of historical droughts in the Amazon region. *Geophys. Res. Lett.*, **38**, L12703, https://doi.org/10.1029/2011GL047436.

McDowell, N. G., and Coauthors, 2015: Global satellite monitoring of climate-induced vegetation disturbances. *Trends Plant Sci.*, **20**, 114–123, https://doi.org/10.1016/j.tplants.2014.10.008.

McKechnie, A. E., P. A. Hockey, and B. O. Wolf, 2012: Feeling the heat: Australian landbirds and climate change. *Emu*, **112**, i–vii, https://doi.org/10.1071/MUv112n2_ED.

McMillan, M., and Coauthors, 2016: A high-resolution record of Greenland mass balance. *Geophys. Res. Lett.*, **43**, 7002–7010, https://doi.org/10.1002/2016GL069666.

Mildrexler, D. J., M. Zhao, F. A. Heinsch, and S. W. Running, 2007: A new satellite-based methodology for continental scale disturbance detection. *Ecol. Appl.*, **17**, 235–250, https://doi.org/10.1890/1051-0761(2007)017[0235:ANSMFC]2.0.CO;2.

——, ——, and S. W. Running, 2009: Testing a MODIS global disturbance index across North America. *Remote Sens. Environ.*, **113**, 2103–2117, https://doi.org/10.1016/j.rse.2009.05.016.

——, ——, and ——, 2011a: A global comparison between station air temperatures and MODIS land surface temperatures reveals the cooling role of forests. *J. Geophys. Res.*, **116**, G03025, https://doi.org/10.1029/2010JG001486.

——, ——, and ——, 2011b: Satellite finds highest land skin temperatures on Earth. *Bull. Amer. Meteor. Soc.*, **92**, 855–860, https://doi.org/10.1175/2011BAMS3067.1.

——, Z. Yang, W. B. Cohen, and D. M. Bell, 2016: A forest vulnerability index based on drought and high temperatures. *Remote Sens. Environ.*, **173**, 314–325, https://doi.org/10.1016/j.rse.2015.11.024.

Mitchell, P. J., A. P. O'Grady, K. R. Hayes, and E. A. Pinkard, 2014: Exposure of trees to drought-induced die-off is defined by a common climatic threshold across different vegetation types. *Ecol. Evol.*, **4**, 1088–1101, https://doi.org/10.1002/ece3.1008.

Moritz, M. A., M.-A. Parisien, E. Batllori, M. A. Krawchuk, J. van Dorn, D. J. Ganz, and K. Hayhoe, 2012: Climate change and disruptions to global fire activity. *Ecosphere*, **3**, 49, https://doi.org/10.1890/ES11-00345.1.

Mu, Q., M. Zhao, J. S. Kimball, N. G. McDowell, and S. W. Running, 2013: A remotely sensed global terrestrial drought severity index. *Bull. Amer. Meteor. Soc.*, **94**, 83–98, https://doi.org/10.1175/BAMS-D-11-00213.1.

Neff, W., G. P. Compo, F. M. Ralph, and M. D. Shupe, 2014: Continental heat anomalies and the extreme melting of the Greenland ice surface in 2012 and 1889. *J. Geophys. Res. Atmos.*, **119**, 6520–6536, https://doi.org/10.1002/2014JD021470.

Nemani, R. R., and S. W. Running, 1997: Land cover characterization using multitemporal red, near-IR, and thermal-IR data from NOAA/AVHRR. *Ecol. Appl.*, **7**, 79–90, https://doi.org/10.1890/1051-0761(1997)007[0079:LCCUMR]2.0.CO;2.

——, L. L. Pierce, and S. W. Running, 1993: Developing satellite derived estimates of surface moisture status. *J. Appl. Meteor.*, **32**, 548–557, https://doi.org/10.1175/1520-0450(1993)032<0548:DSDEOS>2.0.CO;2.

——, S. W. Running, R. A. Pielke, and T. N. Chase, 1996: Global vegetation changes from coarse resolution satellite data. *J. Geophys. Res.*, **101**, 7157–7162, https://doi.org/10.1029/95JD02138.

Nghiem, S. V., and Coauthors, 2012: The extreme melt across the Greenland ice sheet in 2012. *Geophys. Res. Lett.*, **39**, L20502, https://doi.org/10.1029/2012GL053611.

Oyler, J. W., S. Z. Dobrowski, Z. A. Holden, and S. W. Running, 2016: Remotely sensed land skin temperature as a spatial predictor of air temperature across the conterminous United States. *J. Appl. Meteor. Climatol.*, **55**, 1441–1457, https://doi.org/10.1175/JAMC-D-15-0276.1.

Perkins, S. E., L. V. Alexander, and J. R. Nairn, 2012: Increasing frequency, intensity and duration of observed global heatwaves and warm spells. *Geophys. Res. Lett.*, **39**, L20714, https://doi.org/10.1029/2012GL053361.

Pielke, R. A., Sr., and Coauthors, 2007: Unresolved issues with the assessment of multidecadal global land surface temperature trends. *J. Geophys. Res.*, **112**, D24S08, https://doi.org/10.1029/2006JD008229.

Potter, C., P. Tan, M. Steinback, S. Klooster, V. Kumar, R. Myneni, and V. Genovese, 2003: Major disturbance events in terrestrial ecosystems detected using global satellite data sets. *Global Change Biol.*, **9**, 1005–1021, https://doi.org/10.1046/j.1365-2486.2003.00648.x.

Prata, A. J., V. Caselles, C. Coll, J. A. Sobrino, and C. Ottlé, 1995: Thermal remote sensing of land surface temperature from satellites: Current status and future prospects. *Remote Sens. Rev.*, **12**, 175–224, https://doi.org/10.1080/02757259509532285.

Rebetez, M., O. Dupont, and M. Giroud, 2009: An analysis of the July 2006 heatwave extent in Europe compared to the record year of 2003. *Theor. Appl. Climatol.*, **95**, 1–7, https://doi.org/10.1007/s00704-007-0370-9.

Rockström, J., and Coauthors, 2009: Planetary boundaries: Exploring the safe operating space for humanity. *Ecol. Soc.*, **14**, 32, https://doi.org/10.5751/ES-03180-140232.

Saatchi, S., S. Asefi-Najafabady, Y. Malhi, L. E. O. C. Aragao, L. O. Anderson, R. B. Myneni, and R. Nemani, 2013: Persistent effects of a severe drought on Amazonian forest canopy. *Proc. Natl. Acad. Sci. USA*, **110**, 565–570, https://doi.org/10.1073/pnas.1204651110.

Sandholt, I., K. Rasmussen, and J. Andersen, 2002: A simple interpretation of the surface temperature/vegetation index space for assessment of surface moisture status. *Remote Sens. Environ.*, **79**, 213–224, https://doi.org/10.1016/S0034-4257(01)00274-7.

Schubert, S. D., H. Wang, R. D. Koster, M. J. Suarez, and P. Y. Groisman, 2014: Northern Eurasian heat waves and droughts. *J. Climate*, **27**, 3169–3207, https://doi.org/10.1175/JCLI-D-13-00360.1.

Schwalm, C. R., and Coauthors, 2012: Reduction in carbon uptake during turn of the century drought in western North America. *Nat. Geosci.*, **5**, 551–556, https://doi.org/10.1038/ngeo1529.

Seneviratne, S. I., M. G. Donat, B. Mueller, and L. V. Alexander, 2014: No pause in the increase of hot temperature extremes. *Nat. Climate Change*, **4**, 161–163, https://doi.org/10.1038/nclimate2145.

Shaposhnikov, D., and Coauthors, 2014: Mortality related to air pollution with the Moscow heat wave and wild fire of 2010. *Epidemiology*, **25**, 359–364, https://doi.org/10.1097/EDE.0000000000000090.

Sinclair, J. G., 1922: Temperatures of the soil and air in a desert. *Mon. Wea. Rev.*, **50**, 142–144, https://doi.org/10.1175/1520-0493(1922)50<142b:TOTSAA>2.0.CO;2.

Smith, R. C. G., and B. J. Choudhury, 1991: Analysis of normalized difference and surface temperature observations over southeastern Australia. *Int. J. Remote Sens.*, **12**, 2021–2044, https://doi.org/10.1080/01431169108955234.

Steffen, W., P. J. Crutzen, and J. R. McNeill, 2007: The Anthropocene: Are humans now overwhelming the great forces of nature? *Ambio*, **36**, 614–621, https://doi.org/10.1579/0044-7447(2007)36[614:TAAHNO]2.0.CO;2.

Stott, P. A., D. A. Stone, and M. R. Allen, 2004: Human contribution to the European heatwave of 2003. *Nature*, **432**, 610–614, https://doi.org/10.1038/nature03089.

Sulla-Menashe, D., R. E. Kennedy, Z. Yang, J. Braaten, O. N. Krankina, and M. A. Friedl, 2014: Detecting forest disturbance in the Pacific Northwest from MODIS time series using temporal segmentation. *Remote Sens. Environ.*, **151**, 114–123, https://doi.org/10.1016/j.rse.2013.07.042.

Sun, Y., X. Zhang, F. W. Zwiers, L. Song, H. Wan, T. Hu, H. Yin, and G. Ren, 2014: Rapid increase in the risk of extreme summer heat in eastern China. *Nat. Climate Change*, **4**, 1082–1085, https://doi.org/10.1038/nclimate2410.

Tedesco, M., X. Fettweis, M. R. Van den Broeke, R. S. W. Van de Wal, C. J. P. P. Smeets, W. J. Van de Berg, M. C. Serreze, and J. E. Box, 2011: The role of albedo and accumulation in the 2010 melting record in Greenland. *Environ. Res. Lett.*, **6**, 014005, https://doi.org/10.1088/1748-9326/6/1/014005.

Teskey, R., T. Wertin, I. Bauweraerts, M. Ameye, M. A. Mcguire, and K. Steppe, 2015: Responses of tree species to heat waves and extreme heat events. *Plant Cell Environ.*, **38**, 1699–1712, https://doi.org/10.1111/pce.12417.

Teuling, A. J., and Coauthors, 2010: Contrasting response of European forest grassland energy exchanges to heatwaves. *Nat. Geosci.*, **3**, 722–727, https://doi.org/10.1038/ngeo950.

Van De Kerchove, R., S. Lhermitte, S. Veraverbeke, and R. Goossens, 2013: Spatio-temporal variability in remotely sensed land surface temperature, and its relationship with physiographic variables in the Russian Altay Mountains. *Int. J. Appl. Earth Obs.*, **20**, 4–19, https://doi.org/10.1016/j.jag.2011.09.007.

Wan, Z., 2008: New refinements and validation of the MODIS Land-Surface Temperature/Emissivity products. *Remote Sens. Environ.*, **112**, 59–74, https://doi.org/10.1016/j.rse.2006.06.026.

——, Y. Zhang, Q. Zhang, and Z.-L. Li, 2004: Quality assessment and validation of the MODIS global land surface temperature. *Int. J. Remote Sens.*, **25**, 261–274, https://doi.org/10.1080/0143116031000116417.

Wang, H., S. Schubert, R. Koster, Y.-G. Ham, and M. Suarez, 2014: On the role of SST forcing in the 2011 and 2012 extreme U.S. heat and drought: A study in contrasts. *J. Hydrometeor.*, **15**, 1255–1273, https://doi.org/10.1175/JHM-D-13-069.1.

Wendler, G., J. Conner, B. Moore, M. Shulski, and M. Stuefer, 2011: Climatology of Alaskan wildfires with special emphasis on the extreme year of 2004. *Theor. Appl. Climatol.*, **104**, 459–472, https://doi.org/10.1007/s00704-010-0357-9.

Xu, L., A. Samanta, M. H. Costa, S. Ganguly, and R. Nemani, 2011: Widespread decline in greenness of Amazonian vegetation due to the 2010 drought. *Geophys. Res. Lett.*, **38**, L07402, https://doi.org/10.1029/2011GL048049.

Yin, J., J. T. Overpeck, S. M. Griffies, A. Hu, J. L. Russell, and R. J. Stouffer, 2011: Different magnitudes of projected subsurface ocean warming around Greenland and Antarctica. *Nat. Geosci.*, **4**, 524–528, https://doi.org/10.1038/ngeo1189.

Zhao, M., and S. W. Running, 2010: Drought-induced reduction in global terrestrial net primary production from 2000 through 2009. *Science*, **329**, 940–943, https://doi.org/10.1126/science.1192666.

Zhou, L., Y. Tian, S. Baidya Roy, C. Thorncroft, L. F. Bosart, and Y. Hu, 2012: Impacts of wind farms on land surface temperature. *Nat. Climate Change*, **2**, 539–543, https://doi.org/10.1038/nclimate1505.

——, and Coauthors, 2014: Widespread decline of Congo rainforest greenness in the past decade. *Nature*, **509**, 86–90, https://doi.org/10.1038/nature13265.